



## Early and middle Holocene in the Aegean Sea: interplay between high and low latitude climate variability

Gianluca Marino<sup>a,b,\*</sup>, Eelco J. Rohling<sup>c</sup>, Francesca Sangiorgi<sup>a</sup>, Angela Hayes<sup>d</sup>, James L. Casford<sup>e</sup>, André F. Lotter<sup>a</sup>, Michal Kucera<sup>f</sup>, Henk Brinkhuis<sup>a</sup>

<sup>a</sup>Laboratory of Palaeobotany and Palynology, Institute of Environmental Biology, Faculty of Sciences, Utrecht University, Budapestlaan 4, 3584 CD Utrecht, The Netherlands

<sup>b</sup>Institute for Coastal Marine Environment (IAMC), National Research Council (CNR), Porto di Napoli, Calata Porta di Massa, 80133 Naples, Italy

<sup>c</sup>National Oceanography Centre, Southampton, Hampshire SO14 3ZH, United Kingdom

<sup>d</sup>Geography Department, Mary Immaculate College, University of Limerick, Limerick, Ireland

<sup>e</sup>University of Durham, Science Site, South Road, Durham, United Kingdom

<sup>f</sup>Institut für Geowissenschaften, Eberhard-Karls University of Tübingen, Sigwartstrasse 10, DE-72076 Tübingen, Germany

### ARTICLE INFO

#### Article history:

Received 16 January 2009

Received in revised form

13 August 2009

Accepted 18 August 2009

### ABSTRACT

Changes in the orbital parameters, solar output, and ocean circulation are widely considered as main drivers of the Holocene climate. Yet, the interaction between these forcings and the role that they play to produce the pattern of changes observed in different domains of the climate system remain debated. Here, we present new early to middle Holocene season-specific sea surface temperature (SST) and  $\delta^{18}\text{O}_{\text{seawater}}$  results, based on organic-walled dinoflagellate cyst and planktonic foraminiferal data from two sediment cores located in the central (SL21) and south-eastern (LC21) Aegean Sea (eastern Mediterranean). Today, this region is affected by high to mid latitude climate in winter and tropical/subtropical climate in summer. The reconstructed  $\delta^{18}\text{O}_{\text{seawater}}$  from LC21 displays a marked ( $\sim 1.3\%$ ) negative shift between 10.7 and 9.7 ka BP, which represents the regional expression of the orbitally driven African monsoon intensification and attendant freshwater flooding into the eastern Mediterranean. A virtually contemporaneous shift, of the same sign and magnitude, is apparent in the  $\delta^{18}\text{O}_{\text{speleothem}}$  record from Soreq Cave (Northern Israel), an important part of which may therefore reflect a change in the isotopic composition of the moisture source region (Aegean and Levantine Seas). Our SST reconstructions show that Aegean winter SSTs decreased in concert with intensifications of the Siberian High, as reflected in the GISP2 nss  $[\text{K}^+]$  record. Specifically, three distinct sea surface cooling events at 10.5, 9.5–9.03 and 8.8–7.8 ka BP in the central Aegean Sea match increases in GISP2 nss  $[\text{K}^+]$ . These events also coincide with dry interludes in Indian monsoon, hinting at large (hemispheric) scale teleconnections during the early Holocene on centennial timescales. A prominent short-lived ( $\sim 150$  years) cooling event in core SL21 – centred on 8.2 ka BP – is coeval to the ‘8.2 ka BP event’ in the Greenland  $\delta^{18}\text{O}_{\text{ice}}$ , which is commonly linked to a melt-water related perturbation of the Atlantic Meridional Overturning Circulation and associated ocean heat transport. By deciphering the phasing between a recently published record of reduced overflow from the Nordic Seas into the northern North Atlantic, the Greenland  $\delta^{18}\text{O}_{\text{ice}}$  ‘8.2 ka BP event’ anomaly, and the short-lived cooling in SL21, we demonstrate severe far-field impacts of this North Atlantic event in the Aegean Sea. The Aegean is isolated from the North Atlantic oceanic circulation, so that signal transmission must have been of an atmospheric nature.

© 2009 Elsevier Ltd. All rights reserved.

### 1. Introduction

Evidence is mounting from a wealth of globally distributed paleoclimate archives that the climate of the current interglacial

period (the Holocene, since  $\sim 11.6$  ka BP) has been mainly modulated by changes in the solar input, which are attributable to both changes in the Earth’s orbital parameters (long-term) and in the solar activity (short-term) (Mayewski et al., 2004). The orbitally driven enhanced summer insolation of the early Holocene controlled the stepwise retreat of the Laurentide Ice Sheet, the largest Northern Hemisphere ice sheet during the last glaciation (Clark et al., 1999), leading to its final demise at  $\sim 6.8$  ka BP (Carlson et al., 2008). At low latitudes, the insolation increase during the

\* Corresponding author. Present address: Universitat Autònoma de Barcelona (UAB), Institut de la Ciència i de la Tecnologia Ambientals (ICTA), Edifici Cn, Campus UAB, 08193 Bellaterra (Cerdanyola del Vallès), Spain. Tel.: +34 93 581 2488; fax: +34 93 581 3331.

E-mail address: [gianluca.marino@uab.cat](mailto:gianluca.marino@uab.cat) (G. Marino).

earliest Holocene promoted a northward shift of the mean latitudinal position of Intertropical Convergence Zone (ITCZ), a marked intensification of the boreal summer monsoon, and, in turn, considerable changes in the hydrological cycle (e.g., An et al., 2000; deMenocal et al., 2000; Gasse, 2000; Haug et al., 2001; Fleitmann et al., 2007; Weldeab et al., 2007). On shorter timescales, Holocene centennial- to millennial-scale climate perturbations appear to coincide with intervals of reduced solar activity, as inferred from the cosmogenic isotope records (e.g., Denton and Karlén, 1973; O'Brien et al., 1995; Bond et al., 2001; Neff et al., 2001; Rohling et al., 2002; Mayewski et al., 2004; Maasch et al., 2005; Mangini et al., 2007).

Superimposed on the orbital to multi-centennial patterns of climate variability, there has been at least one short-lived (~160 years) abrupt cooling episode, the so-called '8.2 ka BP event' (for overviews see Alley and Ágústssdóttir, 2005; Rohling and Pälike, 2005; Thomas et al., 2007). This climate event, which may have even extended outside the North Atlantic region across the Northern Hemisphere, has been attributed to collapse of oceanic northward heat transport due to slow-down of the Atlantic Meridional Overturning Circulation (AMOC), in response to an outburst of glacial melt-water into the northern North Atlantic (for key observations and interpretations, see, e.g., Alley et al., 1997; Barber et al., 1999; Alley and Ágústssdóttir, 2005; Rohling and Pälike, 2005; Ellison et al., 2006; LeGrande et al., 2006; Wiersma and Renssen, 2006; Rasmussen et al., 2007; Kleiven et al., 2008). Recently, Fleitmann et al. (2008) reported evidence for another such cooling episode, which is centred on ~9.2 ka BP and may also have been triggered by a glacial melt-water injection into the North Atlantic.

Rohling and Pälike (2005) collated data for the '8.2 ka BP event', and argued that this short-lived anomaly: (a) had a considerable winter-weighted character, and (b) was superimposed upon a multi-centennial climate change. Accordingly, they called for season-specific and chronologically carefully constrained proxy reconstructions to trace the true extent of the short-lived anomaly, and thus advance our understanding of the impacts of AMOC reductions on the wider Northern Hemisphere climate. The present study follows the approach of establishing – through the early to middle Holocene period – co-registered summer- and winter-specific proxy records from the Aegean Sea (north-eastern Mediterranean), a key region that is sufficiently distant and isolated from the North Atlantic not to be directly affected by its oceanic circulation. Importantly, the Aegean climate reflects high- and low-latitude influences on the winter and summer regimes, respectively (see Section 2). Thus, Aegean season-specific proxy records presented here, besides elucidating the regional and seasonal climate responses to the early Holocene melt-water-forced AMOC reduction(s), may provide a comprehensive portrayal of the phasing of the multi-centennial pattern of climate variability versus the underlying insolation driven changes in the wider tropical/subtropical realm.

By compiling a variety of season-specific, highly resolved sea-surface proxy records, which are co-registered within the same archive/sample-set, we reconstruct changes in winter and summer sea-surface temperature and hydrographic regimes in the Aegean Sea during the early to middle Holocene period. The paleoceanographic proxies employed are: qualitative winter sea surface temperature (SST) reconstructions based on organic-walled dinoflagellate cyst (dinocyst) abundances; quantitative (artificial neural network, ANN, see Hayes et al., 2005) summer- and winter-SST reconstructions based on planktonic foraminiferal census counts; and hydrographic reconstructions based on planktonic foraminiferal oxygen isotope ( $\delta^{18}\text{O}$ ) data that, together with the ANN SST data, yield seawater  $\delta^{18}\text{O}$ . Finally, to assess causal relationships and

decipher larger (hemispheric) scale climate interactions, we discuss our (season-specific) Aegean Sea reconstructions with key paleoclimate proxy records from the Northern Hemisphere, namely Greenland (Groote et al., 1993; Mayewski et al., 1997; Rasmussen et al., 2007), the northern North Atlantic (Ellison et al., 2006; Kleiven et al., 2008), Northern Israel (Soreq Cave) (Bar-Matthews et al., 2000) and Southern Oman (Qunf Cave) (Fleitmann et al., 2003) (Fig. 1a).

## 2. Rationale and regional setting

The Aegean Sea is distant and practically isolated from the North Atlantic oceanic circulation (Fig. 1a). Previous work has shown that it is highly sensitive to high-latitude climate changes, through an intense atmospheric connection related to the meridional extent of the atmospheric polar vortex (Rohling et al., 2002; Casford et al., 2003 and references therein). Timing and magnitude of the sea surface cooling events in the Aegean are here investigated to assess if, besides the centennial- to millennial-scale climate fluctuations that are possibly tied to decreased solar activity (Rohling et al., 2002), there exists any evidence of change correlative to the '8.2 ka BP event' in this region, thereby testing the model-suggested atmospheric downstream impacts of melt-water related AMOC reductions (e.g., LeGrande et al., 2006; Wiersma and Renssen, 2006). Focusing on the underlying orbitally driven changes, planktonic foraminiferal  $\delta^{18}\text{O}$  records for Aegean Sea sediment cores indicate that surface-water  $\delta^{18}\text{O}$  is predominantly influenced by changes in the eastern Mediterranean's overall freshwater budget, which is modulated by fluctuations in the strength of the African monsoon (Rohling, 1999; Casford et al., 2002, 2003; Rohling et al., 2002, 2004; Marino et al., 2007).

The present-day winter regime in the Aegean Sea is dominated by westerly circulation, which drives a net eastward transport of Mediterranean depressions towards Turkey and the Levant, following their formation by cyclogenesis that takes place over the northern sectors of the relatively warm Mediterranean basin (for overviews, see Rohling and Hilgen, 1991; Lionello et al., 2006; Rohling et al., 2009). Occasionally, particularly dry and cold polar/continental air masses break out over the basin through gaps in the mountainous southern European margin, determining episodes of severe cooling (for overviews, see Maheras et al., 1999; Casford et al., 2003; Rohling et al., 2009). Reconstructions of Aegean climate during the Holocene have revealed the occurrence of these episodes of exceptional winter cooling also on multi-centennial to millennial timescales, with a strong apparent link to concomitant intensifications of the atmospheric polar vortex (Rohling et al., 2002; Casford et al., 2003).

Today, summer conditions in the wider eastern Mediterranean are dominated by expansion of subtropical atmospheric cell from the south, and although there is some cyclogenesis over the basin, little precipitation develops as a consequence of descent in the upper troposphere (Rodwell and Hoskins, 1996; Ziv et al., 2004; Lionello et al., 2006; Rohling et al., 2009).

The eastern Mediterranean climate strongly influences the physical parameters of the surface water masses, leading to increasing densities, which play a central role in the functioning of the thermohaline circulation of the entire Mediterranean basin (e.g., Pinardi and Masetti, 2000). Surface waters from the western basin enter the Levantine Sea via the Strait of Sicily and subsequently circulate along the coasts of Northern Africa, Middle East and Turkey, following a large-scale counter-clockwise path that terminates in the Rhodes gyre where formation of Levantine intermediate waters occurs (Pinardi and Masetti, 2000) (Fig. 1b). Levantine warm (~16 °C in winter, >23 °C in summer), highly saline (~39 psu) surface and intermediate waters subsequently

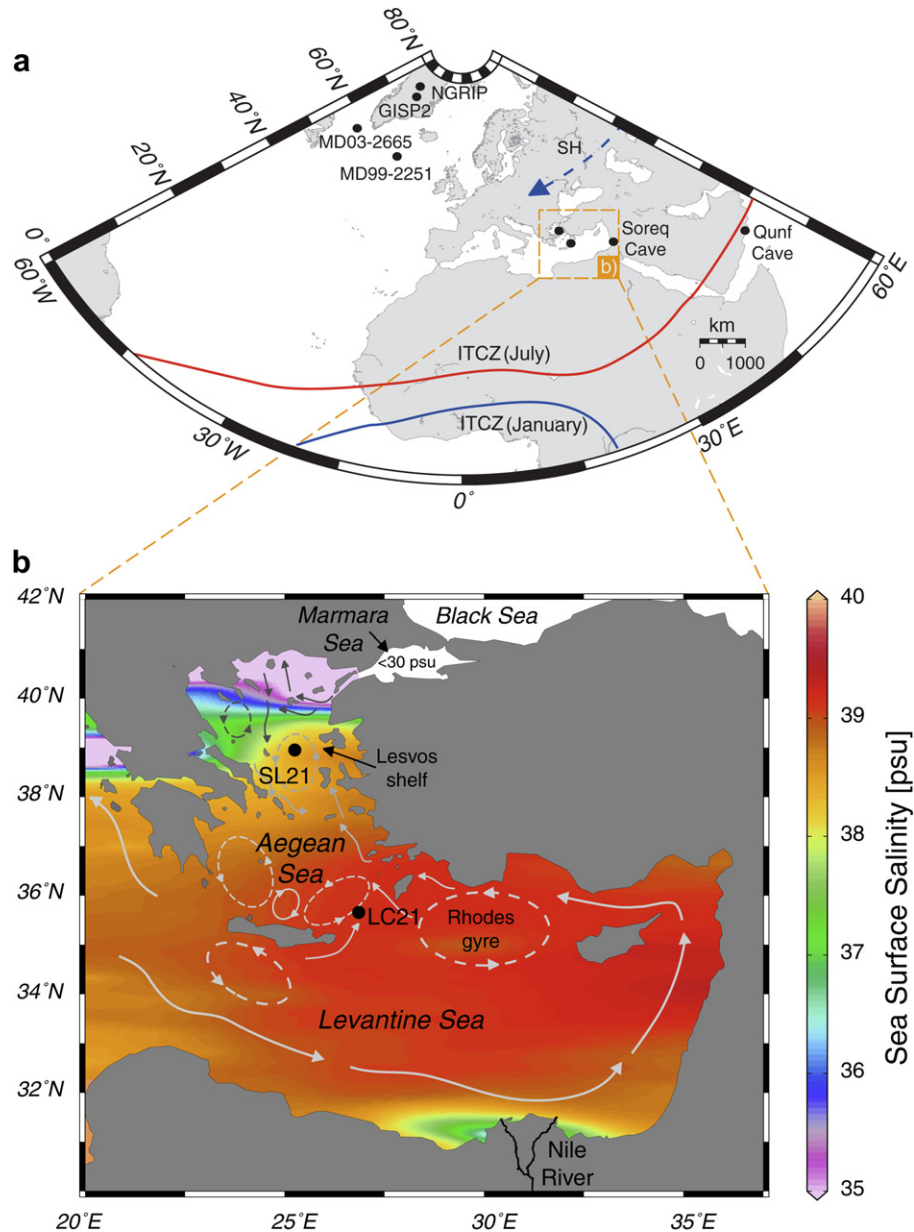


**Fig. 1.** Location of the sites discussed in the text. a) Greenland Summit (GISP2 and NGRIP ice cores), the North Atlantic (MD03-2665 and MD99-2251 sediment cores), the Aegean Sea, and the Middle East (speleothems from Soreq and Qunf Caves). Blue and red solid lines indicate the present-day mean latitudinal position of the Intertropical Convergence Zone (ITCZ) in January and July, respectively. The blue dashed arrow tracks the westward ridging of the Siberian High (SH) towards northwest Europe and southern Scandinavia during winter/spring. b) Inset shows location of the Aegean sediment cores LC21 and SL21 and the main patterns of sea surface-water circulation (grey arrows), cyclonic (solid circles) and anticyclonic gyres (dashed grey circles) in the Levantine and Aegean Seas (Pinardi and Masetti, 2000; Lykousis et al., 2002). Map contours show sea surface salinities (practical salinity units, psu) (MEDAR Group, 2002). (For interpretation of the references to colour in this figure legend, the reader is referred to the web version of this article.)

enter the Aegean Sea through straits in the south-eastern sector of the basin (Cretan Sea), and progress northward along the western coast of Turkey, where their salinity remains roughly unchanged while temperatures become as low as 14.5 °C in winter (22 °C in summer) (Poulos et al., 1997; Zervakis et al., 2004; Gertman et al., 2006). North of the Lesvos shelf, these southern-derived waters form a pronounced thermohaline front with the relatively fresh (<38.0 psu) and cold (<13 °C) Northern Aegean waters that contain considerable admixtures of much fresher waters that originate from the Black Sea/Marmara Sea (24–28 psu) (Zervakis et al., 2004; Gertman et al., 2006). Vigorous cyclonic circulation in the central Aegean governs the location of this front, which bends and directs southward along the eastern coast of Greece (Zervakis et al., 2004),

fuelling relatively low salinity waters (38.8 psu) in the south-western Aegean (Lykousis et al., 2002).

During the orbitally induced insolation/monsoon maximum of the early to middle Holocene, the influence of the African summer monsoon on the eastern Mediterranean was enhanced through intensified flooding especially of the Nile River, which weakened the basin's thermohaline circulation leading to sapropel S1 deposition (Rossignol-Strick et al., 1982; Fontugne et al., 1994; Rohling and De Rijk, 1999; Emeis et al., 2000; Scrivner et al., 2004). Recent pollen-based reconstructions indicate concomitant increase in winter precipitation over the northern borderlands of the Aegean Sea (Kotthoff et al., 2008). Speleothem  $\delta^{18}\text{O}$  data from Soreq Cave in Northern Israel are interpreted as indicative of enhanced

precipitation during the same interval, although this could not be seasonally specified (Bar-Matthews et al., 2000). Combined oxygen and hydrogen isotope data in fluid inclusions within the speleothems suggest that at that time (as today) the moisture originated from the eastern Mediterranean (Matthews et al., 2000; McGarry et al., 2004). Reconstructions from stable oxygen isotopes in snail shells in the Negev Desert, southern Israel, corroborate the persistence of Mediterranean sourcing for the moisture that precipitated over the Levant (Goodfriend, 1991).

The above implies that, by reconstructing early to middle Holocene season-specific temperature and hydrographic changes in the Aegean Sea, we should be able to decipher shifts in key components of the Northern Hemisphere climate, namely the atmospheric polar vortex and the boreal (African) summer monsoon.

### 3. Materials and methods

Descriptions of Aegean cores LC21 (Cretan Sea; 35°40'N; 26°35'E; 1522 m water depth) and SL21 (Lesvos shelf, 39°01'N; 25°25'E; 317 m water depth) (Fig. 1b) are given in Casford et al. (2002, 2003). Both cores contain distinct organic-rich dark intervals representing the regional expression of sapropel S1 (Mercone et al., 2000, 2001; Casford et al., 2002, 2003; Rohling et al., 2002). Cores SL21 and LC21 were sampled in contiguous sequences of 0.5 and 1 cm intervals, respectively, which allows investigation of the early to middle Holocene at multi-decadal to centennial resolution.

#### 3.1. Palynological processing

Samples for dinocyst analyses were oven-dried at 60 °C and spiked with *Lycopodium clavatum* spores. Weighted sediment samples (~0.5 to ~2 g) were treated with 10% cold HCl to remove carbonates, 38% cold HF to remove silicates, and 30% cold HCl to remove the fluoride gel. After sieving over a 10 µm nylon mesh sieve, aliquots (40–60 µl) of the homogenized residue were placed on microscope slides, embedded in glycerine jelly and sealed with paraffin wax. The slides were entirely counted for dinocyst abundances (~250 cysts per sample) at 400× magnification. The taxonomy follows Fensome and Williams (2004) and Rochon et al. (1999). For the purpose of the present study, the abundance of one dinocyst species (*Spiniferites elongatus*) was selected to reconstruct relative changes in the sea surface temperature in core SL21 (see Section 4.2). The complete dinocyst assemblage dataset for core SL21 is available upon request.

#### 3.2. SST reconstruction from planktonic foraminiferal abundances

Planktonic foraminifera census counts from core LC21 (De Rijk et al., 1999; Hayes et al., 1999; Casford et al., 2002) were converted into summer and winter SSTs using artificial neural networks (ANNs) developed for application in the Mediterranean Sea (Hayes et al., 2005). ANN is a computer-intensive approach based on unsupervised learning of a relationship between two sets of variables. In comparison with other transfer function techniques, ANN has the ability to characterise highly non-linear relationships and extract general relationships even from relatively small calibration datasets (Malmgren et al., 2001). Hayes et al. (2005) used ten different partitions of the calibration dataset into training and validation subsets to obtain ten neural networks for each SST definition. The reconstructed SSTs are then calculated as averages of SST estimates from these ten networks and the divergence among the ten estimates is used to estimate the reliability of each SST reconstruction. In the calibration by Hayes et al. (2005), the census counts were calibrated to winter (JFM) and summer (JAS) long-term SST averages at 10 m depth and calibration errors, expressed

as average root mean square errors of prediction (RMSEP) in the test set of each of the ten partitions, were 1.14 °C for summer and 0.79 °C for winter SSTs.

#### 3.3. Chronological framework

The chronology of several Aegean Sea sediment cores, including LC21 and SL21, was established in a multi-proxy correlation framework that relies on a total of more than 30 accelerator mass spectrometry (AMS) radiocarbon (<sup>14</sup>C) datings (Casford et al., 2007). Crucially, the approach proposed by Casford et al. (2007) is particularly robust within the early to middle Holocene interval focus of our study because of the reduced deep-sea ventilation (sapropel S1 deposition) that virtually suppresses bioturbation.

South-East Aegean core LC21 is the benchmark against which Casford et al. (2007) constructed/honed the chronologies of other Aegean cores. The LC21 chronology is itself based on 8 AMS <sup>14</sup>C dating points (solid blue dots in Fig. 2a) (Mercone et al., 2000), and these are supplemented by 3 additional datings from the multi-proxy correlation framework (open blue dots in Fig. 2a) (Rohling et al., 2002; Casford et al., 2007). Radiocarbon ages have been calibrated using CALIB 5.0.2 (Stuiver and Reimer, 1993) and the MARINE04 calibration dataset (Hughen et al., 2004). Different local reservoir age corrections ( $\Delta R$ ) were used for the Lateglacial ( $\Delta R = 420 \pm 120$  years, Siani et al., 2001), sapropel ( $\Delta R = 149 \pm 30$  years, Facorellis et al., 1998), and non-sapropel ( $\Delta R = 58 \pm 85$  years, Reimer and McCormac, 2002) intervals. The goodness of fit of the polynomial regression, upon which the LC21 age/depth relationships are based, is expressed using  $1\sigma$  confidence bounds in Fig. 2a. The majority of calibrated <sup>14</sup>C datings falls either on, or well within, the  $1\sigma$  confidence limits. Furthermore, we identify 5 'tie-points' between the LC21 and GISP2 chronologies (Meese et al., 1997) through the early to middle Holocene (see Fig. S1 in the Supplementary material), based on visual graphic correlation between structural similarities in the GISP2 non-seasalt potassium record and the LC21 warm- versus cold-water planktonic foraminiferal ratio (Rohling et al., 2002). The three early Holocene tie-points fall all well within the  $1\sigma$  bounds of our polynomial regression through the calibrated <sup>14</sup>C datings, with an offset between LC21 and GISP2 chronologies that amounts, at most, to ~150 years (Fig. S1). This supports the robustness of our chronology in this crucial segment of the record. Between 7 and 5 ka BP, the  $1\sigma$  limits embed neither the tie-points nor all the LC21 dating points, with an inferred offset from the GISP2 chronology of more than 600 years between 6.7 and 6 ka BP (Fig. S1). Notably, this interval does coincide with increases both in the percentage of oxygen-requiring benthic foraminifera, and in the concentrations of total benthic foraminifera in LC21 (cf. Fig. 1 in Mercone et al., 2001), which mark the resumption of deep-water ventilation that terminated the deposition of sapropel S1. Injection of new deep waters into the water column, and associated upward advection of 'old carbon' from the interior of the basin, may have increased the reservoir age of surface waters, thereby producing the apparently 'too old' LC21 AMS <sup>14</sup>C-based chronology in this interval (Fig. S1). For the late Holocene, we note that the '-350 years correction' proposed by Rohling et al. (2002) on the basis of the Minoan eruption of Santorini implies chronological shifts within the  $1\sigma$  confidence limits around our regression (Fig. 2a).

The above implies that our calibrated AMS <sup>14</sup>C chronology for core LC21 is accurate within few centuries ( $1\sigma = \pm 417$  years) throughout the Holocene. Notably, in the early Holocene it is 'too old' by, at most, ~150 years relative to the GISP2 chronology, which has itself an estimated error of 2% in that interval (Meese et al., 1997). Chronology for central Aegean core SL21 was obtained by transferring the SL21 records onto an LC21-equivalent-depth scale

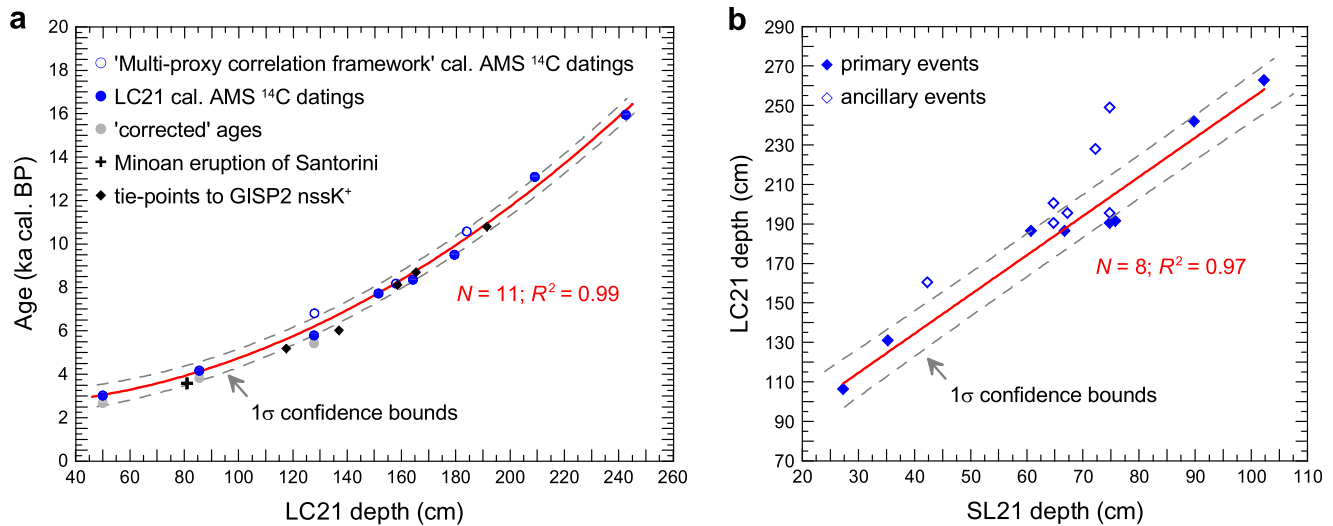


**Fig. 2.** Chronological framework for Aegean Sea cores LC21 and SL21. (a) LC21 depth scale adjusted for the 10 cm thickness of the Minoan ash layer of Santorini plotted versus calibrated ages (for details see Mercone et al., 2000; Rohling et al., 2002). Dashed grey lines represent the  $1\sigma$  confidence intervals of the second order polynomial fit (red solid line) through all calibrated AMS  $^{14}\text{C}$  dating points (blue solid and open dots) upon which chronology is based. Grey solid circles are the AMS  $^{14}\text{C}$  calibrated ages "corrected" to match the actual age of ash layer of the Minoan eruption of Santorini (black cross) (Rohling et al., 2002). Solid black diamonds are the tie-points used to compare the LC21 chronology to the GISP2 age scale. (b) Linear fit through the primary correlation events (blue solid and open diamonds) identified by Casford et al. (2007) to transfer the SL21 depth scale onto the LC21 depth scale and, in turn, to provide a chronological framework for core SL21. Dashed grey lines represent the  $1\sigma$  confidence bounds of the linear regression (solid red line). (For interpretation of the references to colour in this figure legend, the reader is referred to the web version of this article.)

on the basis of the multi-proxy correlation approach of Casford et al. (2007) (Fig. 2b), and by subsequently applying the LC21 depth/age relationship as shown in Fig. 2a.

The developed chronology for the Aegean records allows us to discuss timing relationships with climate signals obtained from other well-dated, highly resolved archives, namely the Greenland ice cores (Meese et al., 1997; Rasmussen et al., 2007), and the Th/U-dated speleothem record from Southern Oman (Qunf Cave) (Fleitmann et al., 2007). All records discussed in this paper are considered in calibrated (cal.) age in kiloyears (ka) before present (BP, which refers to the conventional benchmark of 1950 AD).

In the fine-scale assessment of the early Holocene North Atlantic climate and ocean variability, we use all ice-core records against the new layer-counted GICC05 timescale. To transfer the early Holocene GISP2 oxygen isotope and ion series onto the GICC05 timescale, 19 'matching-points' were used between the two ice cores' electrical conductivity measurements (see Rasmussen et al., 2008) (Fig. S2).

#### 4. Paleoclimate proxy records

##### 4.1. The high-latitude climate signal: Greenland ice cores

Greenland records considered here are the oxygen isotopes ( $\delta^{18}\text{O}_{\text{ice}}$ ), marine-sourced seasalt sodium (ss [ $\text{Na}^+$ ]), and continental-sourced non-seasalt potassium (nss [ $\text{K}^+$ ]) ion concentrations from the well-dated (Meese et al., 1997), finely resolved Greenland Ice core Project Two (GISP2) ice core (Fig. 1) (Grootes et al., 1993; Mayewski et al., 1997). For the early Holocene, the  $\delta^{18}\text{O}_{\text{ice}}$  record of the North Greenland Ice core Project (NGRIP) ice core (Fig. 1) (NGRIP members, 2004) complements the GISP2  $\delta^{18}\text{O}_{\text{ice}}$  reconstruction, using the latest, layer-counted GICC05 timescale (Rasmussen et al., 2007).

Down-core  $\delta^{18}\text{O}_{\text{ice}}$  fluctuations predominantly reflect past changes in temperature (Dansgaard, 1964) and dynamics of the air masses advected over Greenland (Charles et al., 1994). Cooling (warming) results in the shift to lighter (heavier)  $\delta^{18}\text{O}_{\text{ice}}$  values

(Dansgaard, 1964; Dansgaard et al., 1989). Increases (decreases) in the GISP2 ss [ $\text{Na}^+$ ] closely reflect deepening (shallowing) of the Icelandic Low (Meeker and Mayewski, 2002). Increases (decreases) in the nss [ $\text{K}^+$ ] time series from GISP2 have been found to covary with periods of winter/spring strengthening (weakening) of the Siberian anticyclone, the coldest and densest air mass in the Northern Hemisphere (Mayewski et al., 1997; Cohen et al., 2001; Meeker and Mayewski, 2002).

##### 4.2. Season-specific reconstructions of Aegean climate variability: dinocysts and planktonic foraminifera

Dinoflagellates thrive in the upper photic zone and some of them produce fossilizable cysts, which can be preserved in the sediment record (e.g., Taylor, 1987). Several studies, based on surface sediment samples, have revealed clear links between the occurrence of a certain dinocyst species and sea-surface parameters, including temperature (e.g., Rochon et al., 1999; de Vernal et al., 2001; Marret and Zonneveld, 2003). This information has been then applied to the down-core dinocyst records to reconstruct past changes in the sea surface parameters (e.g., de Vernal et al., 2002, 2005). Temperature-sensitive dinocyst species data have provided qualitative SST reconstructions for the eastern Mediterranean, using either calculations of a warm- versus cold-dinocyst ratio ( $W/C_{\text{dinocyst}}$ ) (Sangiorgi et al., 2002), or changes in the relative abundance of warm-water dinocyst assemblages (Sangiorgi et al., 2003).  $W/C_{\text{dinocyst}}$  may be biased due to the systematic dominance of warm taxa in the eastern Mediterranean during the Holocene (Sangiorgi et al., 2003). On the other hand, reconstructions based on cumulative percentages of all warm-water dinocysts may be biased by the different responses of the various warm species to parameters other than temperature, as is often the case with biological proxies (Sangiorgi et al., 2003; Kucera et al., 2005). Here, we reduce the potential for such complications in the assessment of relative SST changes in the eastern Mediterranean by focusing on a single temperature-sensitive species, the cool-water indicator *S. elongatus*.

In the Northern Hemisphere, *S. elongatus* is found in high percentages (up to 50%) in surface samples retrieved from cool temperate to polar regions (mostly where SSTs do not exceed 11 °C and 16 °C in winter and summer, respectively) and reveals no systematic responses to either nutrient availability or salinity (de Vernal et al., 1994; Rochon et al., 1999; Marret and Zonneveld, 2003). In the eastern Mediterranean, this taxon was relatively abundant (up to ~12%) in cold stadials of the last glacial cycle, while it is either found in very low percentages ( $\leq 2\%$ ) or completely absent through the Holocene (Zonneveld, 1995, 1996; Sangiorgi et al., 2002). Aegean summer SSTs are much higher than 16 °C today (Section 2) as well as in the early to middle Holocene of maximum summer insolation (see following), suggesting that cysts of *S. elongatus* in this region, when present, should most likely reflect a winter-weighted signal. Accordingly, we use shifts in the relative abundance of *S. elongatus* to identify relative winter SST changes through the early to middle Holocene in central Aegean core SL21.

To avoid any bias in the temperature reconstructions and interpretations potentially caused by the high numbers of *Protoperidinium* cysts and their productivity/preservation issues in a sapropel-bearing sequence (for discussions see Zonneveld et al., 2001, 2007; Versteegh and Zonneveld, 2002), we calculate percentages of *S. elongatus* relative to both a total and a gonyaulacoid-only dinocyst sum (for an overview on the gonyaulacoid lineage see Fensome et al., 1993). Differences between these two records would highlight bias in the qualitative SST reconstruction induced by productivity and preservation issues.

Fluctuations in the relative abundance of warm- versus cold-water planktonic foraminifera in south-eastern Aegean core LC21 have been described previously, and were attributed to relative winter SST changes (Rohling et al., 2002). We refer to that study for a detailed discussion.

We supplement these records of relative winter SST changes with absolute summer- and winter-specific SST reconstructions based on the ANN technique using planktonic foraminiferal census counts for core LC21 (De Rijk et al., 1999; Hayes et al., 1999; Casford et al., 2002). The ANN calibration and application to Mediterranean planktonic foraminiferal faunas have been described in detail by Hayes et al. (2005).

#### 4.3. The eastern Mediterranean freshwater budget: Aegean Sea $\delta^{18}\text{O}_{\text{ruber}}$ and $\delta^{18}\text{O}_{\text{seawater}}$

The stable oxygen isotope signature of planktonic foraminiferal calcite ( $\delta^{18}\text{O}_{\text{foraminifera}}$ ) in the eastern Mediterranean is controlled by processes such as the glacial concentration effect on the (modified) Atlantic waters entering the basin, the influence of water temperature on the water to carbonate isotope fractionation, changes in the water residence time in the basin, and changes in the basin's freshwater budget (Rohling, 1999; Rohling et al., 2004). During intervals of sapropel formation, the input of large volumes of isotopically light (monsoon-sourced) freshwater along the North African margin greatly controlled the  $\delta^{18}\text{O}$  of the (eastern) Mediterranean sea surface waters (Rohling, 1999; Rohling and De Rijk, 1999; Rohling et al., 2004; Scrivner et al., 2004; Marino et al., 2007; Osborne et al., 2008). The consequent sea surface freshening has been found to propagate rapidly through the wider eastern Mediterranean away from the sites of freshwater discharge, including the Aegean Sea (Marino et al., 2007), due to the efficient large-scale counter-clockwise circulation of the surface waters (Pinaridi and Masetti, 2000). The south-eastern Aegean site of core LC21 is directly located at the inflow of these surface waters into the Aegean Sea, at a considerable distance 'downstream' from the North African sites of freshwater discharge into the open eastern

Mediterranean (Fig. 1b). Accordingly, the oxygen isotope composition of the surface waters ( $\delta^{18}\text{O}_{\text{seawater}}$ ) at this specific site reflects a well-mixed expression of the changes in the surface-water  $\delta^{18}\text{O}$  in the wider eastern Mediterranean, rather than a merely local signal (Marino et al., 2007).

We reconstruct  $\delta^{18}\text{O}_{\text{seawater}}$  for core LC21 during the early to middle Holocene by combining the stable oxygen isotope record for the (planktonic) summer mixed-layer dwelling foraminifer *Globigerinoides ruber* (white) ( $\delta^{18}\text{O}_{\text{ruber}}$ ) (Rohling et al., 2002) with summer SST reconstructions from ANN calculations within the same sample set of core LC21. Estimates of  $\delta^{18}\text{O}_{\text{seawater}}$  are then derived using the *G. ruber* paleotemperature equation of Bemis et al. (1998):  $\delta^{18}\text{O}_{\text{seawater}} (\text{VSMOW}) = 0.27 + (T (\text{°C}) - 16.5 + 4.8 \times \delta^{18}\text{O}_{\text{ruber}} (\text{VPDB}))$ .

#### 4.4. The tropical and subtropical precipitation signal: speleothem records

Soreq Cave in Northern Israel (Fig. 1a), resides in a semi-arid region where most of the annual rainfall today derives from winter-time Mediterranean cyclogenesis (Bar-Matthews et al., 1996; Matthews et al., 2000). It has been established that the oxygen isotope composition of speleothem calcite ( $\delta^{18}\text{O}_{\text{speleothem}}$ ) in Soreq Cave depends on the annual precipitation and evaporation balance in the epikarst zone, so that lighter (heavier)  $\delta^{18}\text{O}_{\text{speleothem}}$  corresponds to increased (reduced) net precipitation over Soreq Cave (Bar-Matthews et al., 1996).

Qunf Cave (Fig. 1a) is located in Southern Oman at the northern limit of the Indian summer monsoon penetration over the Arabian Peninsula, which accounts for 90% of the annual rainfall in the region (Fleitmann et al., 2003). Given its location, the Qunf Cave  $\delta^{18}\text{O}_{\text{speleothem}}$  record is expected to be very sensitive to even minor shifts of the Intertropical Convergence Zone (ITCZ) and associated Indian summer monsoon (Fleitmann et al., 2003). The so-called 'amount effect' causes the  $\delta^{18}\text{O}$  of precipitation, and consequently speleothem calcite, to shift towards lighter values as rainfall amounts increase (Dansgaard, 1964). Qunf Cave  $\delta^{18}\text{O}_{\text{speleothem}}$  therefore represents a key archive of changes in Indian summer monsoon rainfall.

## 5. Results

### 5.1. The early to middle Holocene monsoon maximum

Our record of ANN-based summer SSTs in LC21 (Fig. 3b) suggest that typical Holocene values were first attained around 10.95 ka BP, and that summer SST was higher than the present-day value of 23.5 °C (Section 2) throughout the early to middle Holocene, which may reflect the orbital boreal summer insolation maximum.

Between 10.7 and 9.7 ka BP, we note a virtually synchronous, rapid decrease of ~1.8‰ of  $\delta^{18}\text{O}_{\text{ruber}}$  in cores LC21 (Fig. 3c) and SL21 (Fig. 3a) and of ~1.4‰ in LC21  $\delta^{18}\text{O}_{\text{seawater}}$  (Fig. 3d). The latter corresponds to 1.26‰ if we account for coeval changes in mean ocean  $\delta^{18}\text{O}$  (Waelbroeck et al., 2002). The close similarity in timing and magnitude of the negative  $\delta^{18}\text{O}$  changes in both foraminiferal calcite (*G. ruber*) and seawater provides strong support to the hypothesis that the negative  $\delta^{18}\text{O}_{\text{ruber}}$  shift in the Aegean cores prior to sapropel S1 deposition is dominated by the inflow of isotopically light fresher surface waters into the Aegean Sea (Casford et al., 2002, 2003) with a negligible role of summer SSTs (i.e., temperature of calcification of *G. ruber* shells). Moreover, this reconstruction suggests that, at least in the early Holocene, fresher surface waters deriving from the South spread as far north as the central Aegean site of core SL21. Advection of fresher surface waters from the North (Kotthoff et al., 2008) is not a likely explanation for the isotope shift

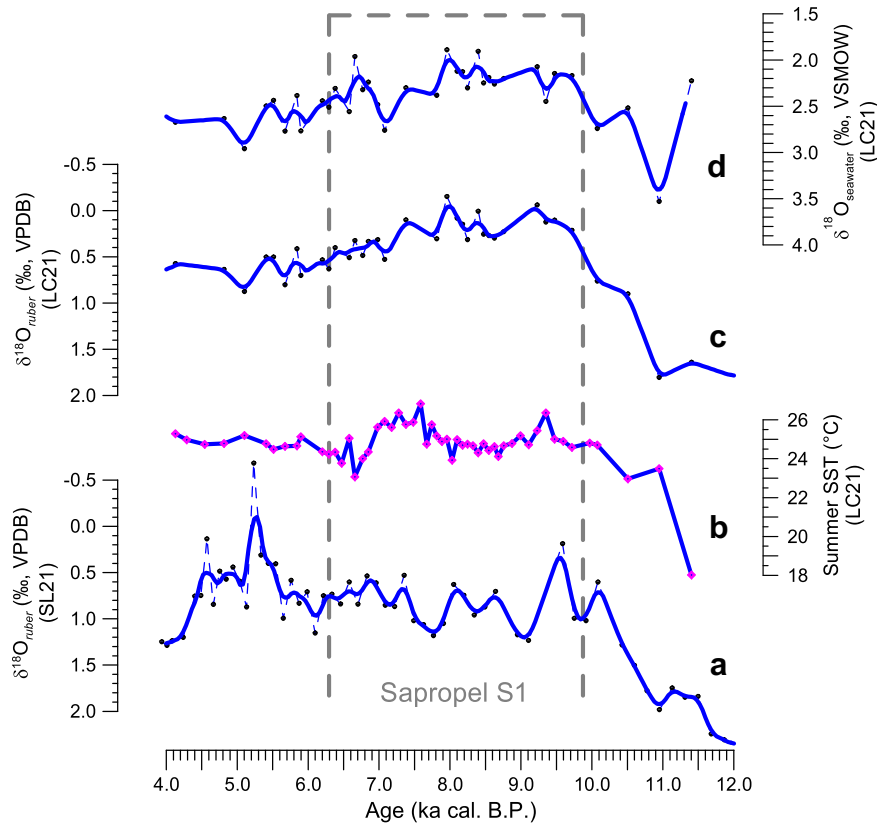


**Fig. 3.** Stable oxygen isotope and summer sea surface temperature (SST) records from Aegean Sea cores SL21 and LC21. Grey dashed lines represent the visual extent of the dark interval associated with the sapropel S1 deposition in the Aegean Sea. (a) and (c)  $\delta^{18}\text{O}$  (‰, VPDB) of the summer mixed-layer dwelling planktonic foraminifer *Globigerinoides ruber* (white) for Aegean Sea cores SL21 and LC21, respectively (Casford et al., 2002, 2003; Rohling et al., 2002). Blue solid lines represent the 200 years moving average across the  $\delta^{18}\text{O}_{ruber}$  profiles. (b) ANN-based summer SSTs for core LC21. The SST axis is calibrated relative to the  $\delta^{18}\text{O}$  axis so that every 1 °C change in temperature corresponds to 0.21‰ in  $\delta^{18}\text{O}$  (Bemis et al., 1998). (d)  $\delta^{18}\text{O}$  (‰, VSMOW) (blue dashed line) and 200 moving average (blue solid line) of sea surface waters at site of core LC21. VPDB – Vienna Pee Dee Belemnite; VSMOW – Vienna Standard Mean Ocean Water. (For interpretation of the references to colour in this figure legend, the reader is referred to the web version of this article.)

in SL21, because of the intense thermohaline front to the north of the core site, which prevents southward extension of the influence of the North Aegean surface waters (Zervakis et al., 2004). The position of this front is controlled by the local cyclonic circulation, which during the early Holocene likely was strong as, or stronger than, today. This is inferred from the evidence in pollen records of increased precipitation over the Aegean borderlands (Kotthoff et al., 2008) and in the Near East (Goodfriend, 1991; Bar-Matthews et al., 2000), which indicates increased activity of Mediterranean depressions with consequently increased cyclonic vorticity input into the basin.

From about 9.6 ka BP onwards, the  $\delta^{18}\text{O}_{ruber}$  records develop rather differently in cores LC21 and SL21. In LC21,  $\delta^{18}\text{O}_{ruber}$  (Fig. 3c) shows low amplitude fluctuations ( $\sim 0.5\text{‰}$ ) around an average of about  $0.15\text{‰}$  until 7.4 ka BP, followed by a gradual increase towards modern values. In core SL21 (Fig. 3a),  $\delta^{18}\text{O}_{ruber}$  values are heavier and more variable. Between 9.1 and 5.7 ka BP, it oscillates around a mean of  $0.7\text{‰}$  which is heavier by  $\sim 0.5\text{‰}$  than the  $\delta^{18}\text{O}_{ruber}$  minimum centred on 9.6 ka BP at the same location. At 5.6 ka BP, SL21  $\delta^{18}\text{O}_{ruber}$  shifts back to lighter values, which then continue until about 4.3 ka BP. We tentatively interpret this negative shift in SL21 as indicative of weakening and/or southward shift of the central Aegean cyclonic cell (and the associated front) and subsequently increased advection of North Aegean waters, which were particularly fresh, following the full reconnection of the Marmara Sea/Black Sea with the Aegean (Sperling et al., 2003; Kuhnt et al., 2007). This is supported by the similarity between the SL21  $\delta^{18}\text{O}_{ruber}$  values and those seen throughout S1 and beyond in the

more western – closer to/under the front – site of core SL31 (Casford et al., 2007). This tentative explanation would agree with middle to late Holocene decrease in precipitation over the Aegean borderlands (decreasing cyclonic activity) after the wet interval coeval to sapropel S1 deposition (Kotthoff et al., 2008).

Comparing the Aegean records with that from Soreq Cave, we note a general ‘bell-shaped’ resemblance in both pattern and magnitude between the LC21  $\delta^{18}\text{O}_{seawater}$  (Fig. 4a) and  $\delta^{18}\text{O}_{speleothem}$  from Soreq Cave (Fig. 4b) (Bar-Matthews et al., 2000) throughout the early to middle Holocene. Both records even display shifts to lighter  $\delta^{18}\text{O}$  that appear virtually contemporaneous – within the chronological uncertainties (Bar-Matthews et al., 2000) – and of similar magnitude.

It has been previously proposed, using an ‘amount effect’ explanation for the light Soreq Cave  $\delta^{18}\text{O}_{speleothem}$  anomaly and on the basis of other geochemical evidence (e.g., Ayalon et al., 1999; Bar-Matthews et al., 1999), that precipitation over Israel was much enhanced between 10 and 7 ka BP, relative to the present (Bar-Matthews et al., 2000). Our records, however, suggest that this notion might need some revision, given that deuterium excess values of fluid inclusions in the speleothems imply that precipitation over Soreq Cave at that time (as today) was sourced from the eastern Mediterranean (Matthews et al., 2000; McGarry et al., 2004). Based on the rather similar developments of LC21  $\delta^{18}\text{O}_{seawater}$  and Soreq Cave  $\delta^{18}\text{O}_{speleothem}$  (Fig. 4b) we suggest that the speleothem data to a considerable degree may reflect an overall  $\delta^{18}\text{O}$  change in the source for the eastern Mediterranean vapour that eventually precipitated over the Levant. Soreq Cave



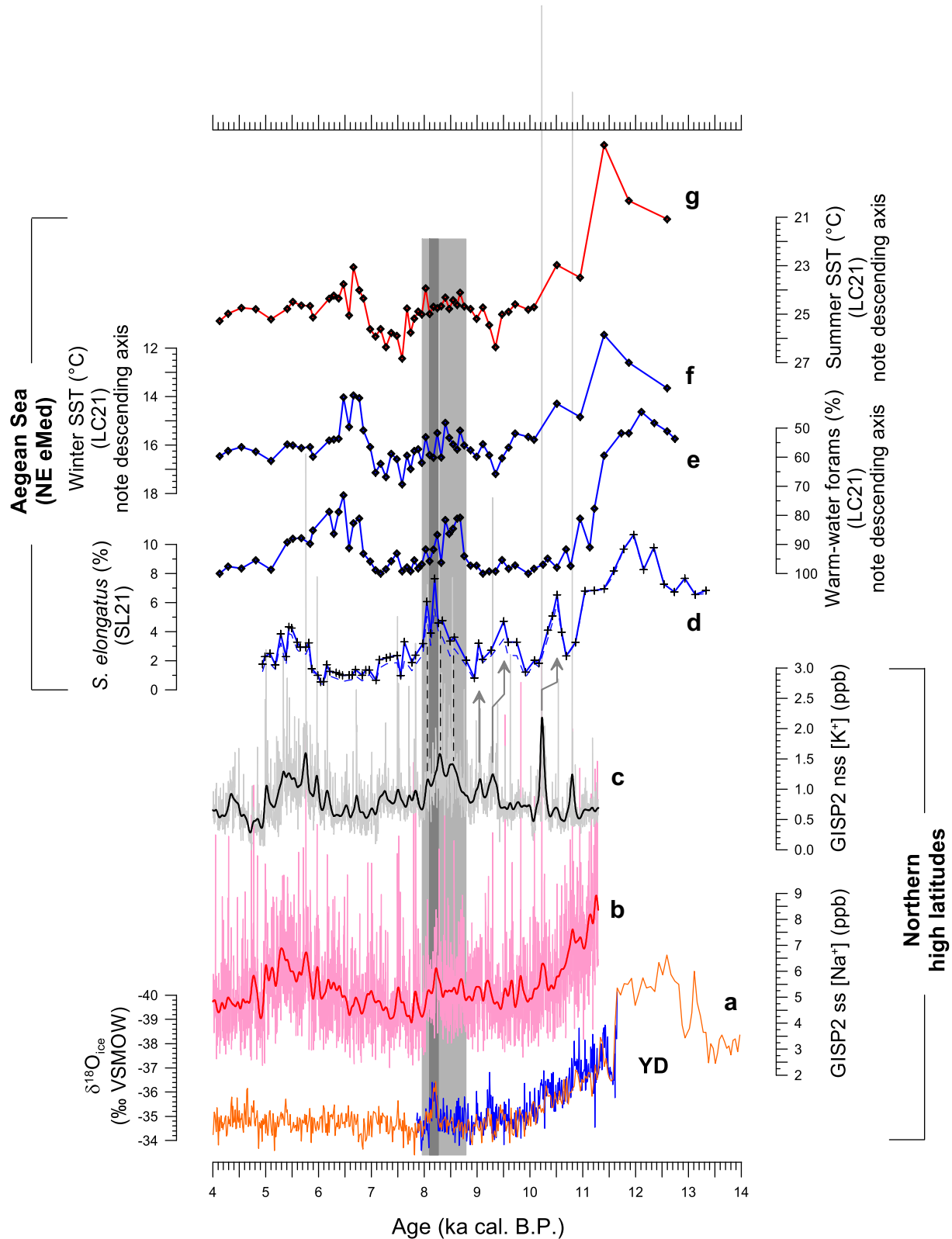


**Fig. 5.** Comparison between Aegean SST and Greenland ice-core records. (a) GISP2 (orange) and NGRIP (blue)  $\delta^{18}\text{O}_{\text{ice}}$  (‰ VSMOW) (Grootes et al., 1993; NGRIP members, 2004).  $\delta^{18}\text{O}_{\text{ice}}$  are presented on their respective timescales (Meese et al., 1997; Rasmussen et al., 2007). (b) GISP2 marine-sourced seasalt sodium series (ss [ $\text{Na}^+$ ], ppb). Red solid line represents a 200-year moving Gaussian to highlight the main trends (Mayewski et al., 1997). (c) GISP2 continental-sourced non-seasalt potassium series (nss [ $\text{K}^+$ ], ppb). Black solid line represents a 200-year moving Gaussian to highlight the main trends (Mayewski et al., 1997). (d) Relative abundances (%) of *Spiniferites elongatus* in core SL21 with respect to a total (blue dashed line) and a gonyaulacoid-only (blue solid line) dinocyst sum. (e) Relative abundances (%) of warm-water planktonic foraminifera for core LC21 (Rohling et al., 2002). (f) ANN-based winter SSTs ( $^{\circ}\text{C}$ ) for core LC21. (g) ANN-based summer SSTs ( $^{\circ}\text{C}$ ) for core LC21. The grey band represents the '8.2 event' in the NGRIP and GISP2  $\delta^{18}\text{O}_{\text{ice}}$ . The light grey band represents the multi-centennial change that embeds this short-lived event (Rohling and Pälike, 2005). Grey arrows and black dashed lines indicate correlative events discussed in the main text. YD = Younger Dryas. (For interpretation of the references to colour in this figure legend, the reader is referred to the web version of this article.)

through this interval between the foraminiferal ratio in core LC21 and the nss GISP2  $[K^+]$  fluctuations.

There is an even more remarkable resemblance between the *S. elongatus* and nss GISP2  $[K^+]$  records within the 8.9–5.0 ka BP interval, both in terms of structure and timing. At 8.8–7.8 and 5.9–5.1 ka BP, the SL21 record of *S. elongatus* also reveals clear expressions of two multi-centennial fluctuations, which were previously reported for core LC21 and related to excursions in the GISP2 nss  $[K^+]$  series (Rohling et al., 2002). In LC21, these changes correspond to winter SST decreases below 15 °C and 14 °C, respectively (Fig. 5f).

Between 8.8 and 7.8 ka BP, changes in the SL21 *S. elongatus* record show a striking signal agreement with a GISP2 nss  $[K^+]$  maximum with the exception of two superimposed sharp *S. elongatus* peaks at 8.2 and 8.05 ka BP. The multi-centennial change in GISP2 nss  $[K^+]$  has been extensively discussed in Rohling et al. (2002), Mayewski et al. (2004), and Rohling and Pälike (2005) and represents part of a repeating pattern of Holocene climate oscillations that might reflect changes in solar activity. The superimposed sharp *S. elongatus* peak centred on 8.2 ka BP stands out as the highest value (~7.7%) attained by this species throughout the early to middle Holocene section of SL21. This short-lived event coincides, with negligible chronological offsets, with the negative  $\delta^{18}O_{ice}$  anomalies found in GISP2 (timescale from Meese et al., 1997) as well as in the new layer-counted (GICC05 timescale) NGRIP record (Rasmussen et al., 2007) (Fig. 5a). We note that these short-lived changes in both the SL21 *S. elongatus* and in the Greenland  $\delta^{18}O_{ice}$  records occur when LC21 winter SSTs and GISP2 nss  $[K^+]$  are – within the context of the underlying longer-term fluctuation – already returning to warmer and lower values, respectively.

Findings reported above corroborate the previous notion of a coherent in-phase response of the Aegean winter climate to the strengthening of the atmospheric polar vortex on multi-centennial to millennial timescales, which may have been modulated by changes in solar irradiation (Rohling et al., 2002; Mayewski et al., 2004). Moreover, the new *S. elongatus* record in SL21 offers information at higher (centennial) resolution, which reveals short-lived superimposed events at 10.5, 9.5, 9.03 and especially at 8.2 ka BP.

## 6. Discussion

### 6.1. Long-term changes in the boreal tropical and subtropical realms

Our new  $\delta^{18}O_{seawater}$  record from south-eastern Aegean core LC21 points to substantial hydrographic changes in the basin during the early to middle Holocene, in agreement with previous reconstructions based on  $\delta^{18}O_{ruber}$  (Casford et al., 2002, 2003). The timing reported here (10.7–9.7 ka BP) for the early Holocene decrease in the  $\delta^{18}O$  of *G. ruber* and seawater in Aegean cores LC21 and SL21 (Fig. 3a, c, and d) coincides with a negative shift (~2.0‰) of  $\delta^{18}O_{ruber}$  in a south-eastern Levantine Sea site close to the Nile River discharge (cf. Fig. 3 of Sperling et al., 2003). These changes in the surface-water  $\delta^{18}O$  appear virtually coeval with a distinct increase of Nile-sourced clay minerals in another south-eastern Aegean sediment core (10.6–9 ka BP) (Ehrmann et al., 2007). The timing of these changes in the Aegean Sea agrees with age estimates for the onset of the so-called “greening of the Sahara” (Ritchie et al., 1985; Gasse, 2000). Combined, these observations corroborate the previous notion that, during the early Holocene, Aegean surface waters freshened primarily in response to the enhanced monsoon-fuelled freshwater flooding into the open eastern Mediterranean (Casford et al., 2002, 2003). We here find that the eastern Mediterranean-wide decrease in surface-water  $\delta^{18}O$  may in turn partly

explain the negative isotope shift in  $\delta^{18}O_{speleothem}$  in Soreq Cave (see Section 5.1, and Fig. 4b).

Taking into account the ~150 year dating uncertainty for LC21 in the earliest Holocene interval (see Section 3.3), the onset of monsoon flooding into the eastern Mediterranean around 10.7 ka BP would appear to lag by at least ~0.8 kyr behind the abrupt shift to wetter conditions (at 11.46 ka BP) in the western Sahel (Weldeab et al., 2007), which is located at the present-day northern edge of the ITCZ penetration over northwest Africa (Ramel et al., 2006). This apparent lag suggests a time-transgressive northward shift of the mean latitudinal position of the monsoon front (in association with the ITCZ) over Northern Africa. Near the eastern equatorial Atlantic, in the north-western Sahel, there would be a direct response of the ITCZ to insolation changes. The delayed northward shift over central and eastern North Africa might then be related to a vegetation-albedo feedback process (Kutzbach et al., 1996; Brovkin et al., 1998), requiring some time for a progressive increase in the vegetation cover following the change to more humid conditions.

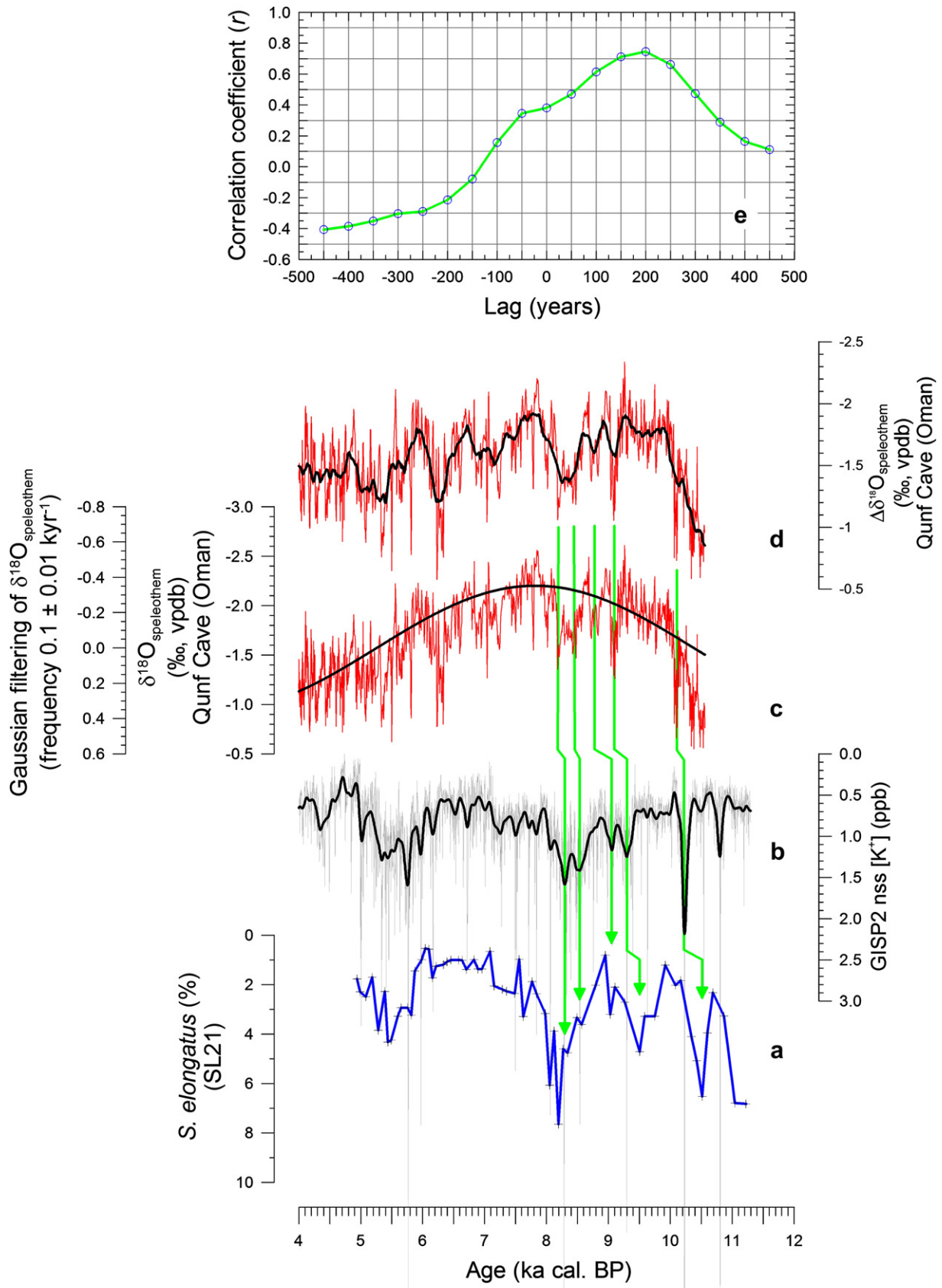
Despite its location on the present-day northernmost limit of the ITCZ (Fleitmann et al., 2003, 2007), the earliest Holocene transition to wetter conditions over Southern Oman at 10.3–9.6 ka BP (Fig. 4c) begins slightly later than the changes in Northern Africa and in the eastern Mediterranean hydrography, and thus lags by up to 1 kyr behind the change in the western Sahel (Weldeab et al., 2007). This suggests a delayed response of the Indian summer monsoon to insolation change, relative to the African monsoon. Such a time lag might be due to a negative relationship between Eurasian snow cover and Indian summer monsoon intensity (Barnett et al., 1988; Fleitmann et al., 2003, 2007; Gupta et al., 2003). Enhanced snow cover over Eurasia reduces the (sensible) heating of the Eurasian landmass, which weakens the pressure gradient between the Indian Ocean and the Tibetan Plateau (Overpeck et al., 1996), the engine of the Indian summer monsoon circulation (Webster et al., 1998).

### 6.2. Centennial- to millennial-scale climate variability in the Aegean Sea and further afield

Our qualitative and quantitative SST reconstructions for the Aegean Sea reveal a distinct pattern of climate deteriorations that in general agrees with the previously reported series of millennial-scale fluctuations in the region (Rohling et al., 2002), but which enriches that picture with centennial-scale details. Overall, winter SST variability in SL21 and to a lesser extent in LC21 show a good match with the GISP2 nss  $[K^+]$  series on all timescales, strengthening the view that the Aegean cooling events represent episodes of enhanced incursion of polar air influences related to intensification of the atmospheric polar vortex (Rohling et al., 2002; Casford et al., 2003). For the early Holocene, however, our new dinocyst-based Aegean winter-specific proxy, the cold-water species *S. elongatus*, reveals a climate evolution that is more complex than was previously appreciated. Two marked climate deteriorations centred on about 10.5 and 9.5–9.03 ka BP have been found in addition to a multi-centennial cooling between 8.8 and 7.8 ka BP that was also reported by Rohling et al. (2002). In the following we discuss these observations in the context of other paleoclimate records from regions distant from the eastern Mediterranean with emphasis on the early Holocene events.

#### 6.2.1. Early Holocene large-scale teleconnections

Within chronological uncertainties, the observed changes in both Greenland and Aegean records (Fig. 6a and b) also agree in both timing and structure with the early Holocene Qunf Cave  $\delta^{18}O_{speleothem}$  record of the Indian summer monsoon, which shows



deteriorations at  $\sim 10.1$  and between 9.3 and 7.9 ka BP in Fig. 6c (Fleitmann et al., 2003). To test this visual similarity, while allowing for minor apparent chronological offsets between the two records, we perform a lagged cross-correlation analysis between the GISP2 nss [K<sup>+</sup>] (Mayewski et al., 1997) and Qunf Cave  $\delta^{18}\text{O}_{\text{speleothem}}$  (Fleitmann et al., 2003) time series through the early to middle Holocene period (Fig. 6e). The Qunf Cave  $\delta^{18}\text{O}_{\text{speleothem}}$  record is first detrended (Fig. 6c) to remove an underlying orbitally paced long-term signal (frequency  $0.1 \pm 0.01 \text{ kyr}^{-1}$ ) (Fig. 6c). Next, we use a lagged cross-correlation test between the 200-year smoothed Qunf Cave  $\delta^{18}\text{O}_{\text{speleothem}}$  residuals and the natural logarithm (see Fig. S4a and b and text in the Supplementary material) of the 200-year moving Gaussian filtered GISP2 nss [K<sup>+</sup>] record (Fig. 6e). This exercise shows that the two time series are positively correlated, sharing 74% (highly significant;  $p = 0.7 \times 10^{-8}$ ) of their variance across the 10.3–8.0 ka BP interval for a lag of 200 years of Qunf Cave  $\delta^{18}\text{O}_{\text{speleothem}}$  behind GISP2 nss [K<sup>+</sup>], which is well within the combined chronological uncertainties (Meese et al., 1997; Fleitmann et al., 2007). Since we here also recognised fluctuations time-equivalent to GISP2 nss [K<sup>+</sup>] events in the Aegean Sea (Fig. 6a), similar to other North Atlantic records (e.g., Bond et al., 1997; von Grafenstein et al., 1999; Björck et al., 2001; Mayewski et al., 2004; Rohling and Pälike, 2005; Ellison et al., 2006; Came et al., 2007; Marshall et al., 2007; Rasmussen et al., 2007; Fleitmann et al., 2008), it appears that the early Holocene climate perturbations may have been virtually synchronous throughout the Northern Hemisphere.

Interestingly, the monsoon record of Fleitmann et al. (2003) might suggest that the (early) Holocene anomalies were not exclusively winter-weighted events (cf. Rohling and Pälike, 2005), but that summer was also affected. We propose a scenario that integrates these observations by inferring a key role for Eurasian snow cover. Besides its aforementioned effects on the Indian summer monsoon, increased Eurasian snow cover would have also been associated with increases in the intensity and spatial extent of the winter Siberian High (Cohen et al., 2001 and references therein). Changes in the Eurasian snow cover may therefore have caused virtually synchronous, yet independent, responses of the winter Siberian High and the summer Indian monsoon systems during the early Holocene. The disappearance of signal similarities between Aegean/GISP2 winter records and the Qunf Cave record after 8.0 ka BP (Fig. 6b and d) may be explained by the eventual development of full interglacial conditions during the middle Holocene, removing this inferred common forcing of high and low latitude systems. Thereafter, the tropics may have responded more directly to variations in the solar activity (Fleitmann et al., 2003; Dykoski et al., 2005). In their review of Holocene climate variability across the globe, Mayewski et al. (2004) also noted that Holocene events after 8 ka BP displayed reasonably common spatial characteristics, whereas earlier events showed different patterns, which corroborates our inference of a change in low- versus high-latitude responses to climate forcing after about 8 ka BP.

### 6.2.2. Phasing of changes in the surface versus deep North Atlantic Ocean waters and in Greenland ice between 8.8 and 7.8 ka BP

We previously noted that the short-lived change at 8.2 ka BP in SL21 and at 8.19 ka BP in NGRIP (Rasmussen et al., 2007) occurred

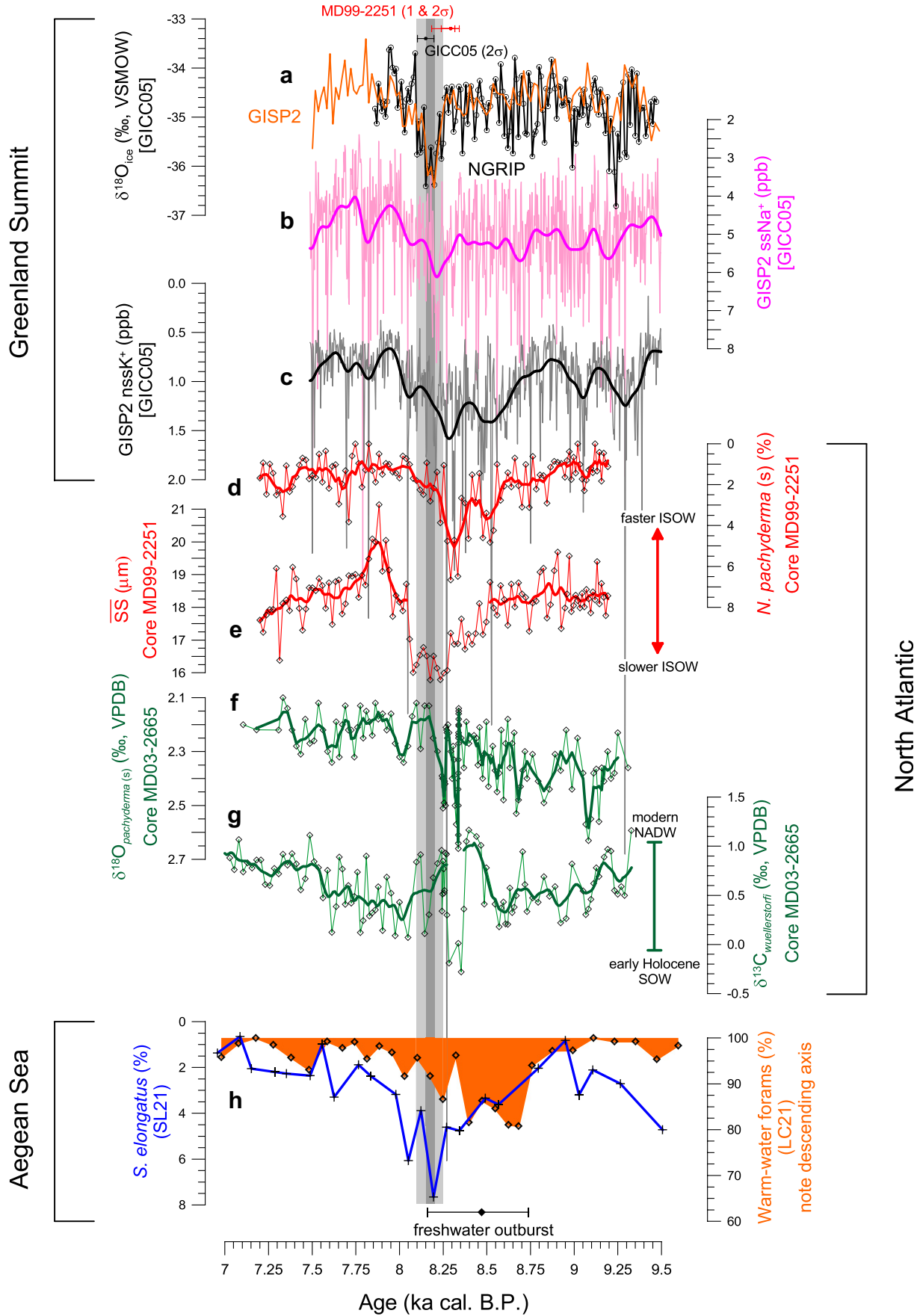
when, following a multi-centennial change, winter SSTs in south-eastern Aegean Sea and dust (potassium) supply to Greenland were increasing and decreasing, respectively. We further investigate these interesting phase relationships by comparing the high resolution NGRIP  $\delta^{18}\text{O}_{\text{ice}}$  with the GISP2 nss [K<sup>+</sup>] series. GISP2 records in Fig. 7a–c have been transferred onto the new layer-counted GICC05 chronology (see Section 3.3 and Fig. S2). Fine-scale comparison of NGRIP and GISP2  $\delta^{18}\text{O}_{\text{ice}}$  with GISP2 nss [K<sup>+</sup>] reveals that indeed – similarly to what is shown by the Aegean records (see also Fig. 7h) – the  $\delta^{18}\text{O}_{\text{ice}}$  anomaly occurs when the atmospheric polar vortex begins to weaken towards its Holocene background levels after a multi-centennial maximum. This strongly corroborates the notion that the two events apparent in  $\delta^{18}\text{O}_{\text{ice}}$  and GISP2 nss [K<sup>+</sup>] are indeed differently phased, and thus likely reflect different causal mechanisms (Rohling and Pälike, 2005).

Focusing on the short-lived ‘8.2 ka BP event’ anomaly, model reconstructions convincingly link this event to an AMOC reduction due to a melt-water pulse (e.g., Alley and Ágústssdóttir, 2005; LeGrande et al., 2006; Wiersma and Renssen, 2006), which originated from Hudson Bay at  $8.47 \pm 0.3$  ka BP (Barber et al., 1999). Recently, two multi-proxy records from the northern North Atlantic (core MD99-2251, Gardar Drift, Ellison et al., 2006; core MD03-2665, Erik Drift, Kleiven et al., 2008) have targeted the link between changes in the deep-ocean circulation and the widespread and/or regional cooling around 8.2 ka BP. Both core sites are ideally suited to detect changes in the North Atlantic Deep Water (NADW). Gardar Drift is bathed by Iceland–Scotland Overflow Water (ISOW) (Ellison et al., 2006), while Erik Drift is under the influence of the total integrated Nordic Seas overflow (Hansen and Østerhus, 2000; Hansen et al., 2001; Hunter et al., 2007).

The sortable silt size proxy of deep current flow speed at Gardar Drift (Fig. 7e) points to a gradual decrease in ISOW flow speed between 8.45 and 8.04 ka BP, with an abrupt drop between 8.27 and 8.07 ka BP. Co-registered relative abundances of the polar planktonic foraminiferal species *Neogloboquadrina pachyderma* (s) indicate two increases (interpreted as cooling events) centred on 8.49 and 8.29 ka BP, respectively (Fig. 7d). Taken at face value, the surface- versus deep-ocean phasing in MD99-2251 seems to imply that the main cold event at 8.29 ka BP predates the major ISOW reduction by a few decades, in disagreement with the sequence of events predicted by models (e.g., Alley and Ágústssdóttir, 2005; LeGrande et al., 2006; Wiersma and Renssen, 2006).

Ellison et al. (2006) interpret the *N. pachyderma* (s) event centred on 8.29 ka BP as the SST counterpart of the Greenland  $\delta^{18}\text{O}_{\text{ice}}$  anomaly (Fig. 6a) and ascribe the apparent age offset to combined chronological uncertainties in the two records, rather than to an actual phase lag. Notably, this conclusion overlooks the absence of straightforward structural similarities of the two records in the intervals preceding and following the event. Furthermore, when the  $\delta^{18}\text{O}_{\text{ice}}$  is considered on the GICC05 timescale, the offset with the MD99-2251 cooling event becomes slightly larger ( $\sim 143$  years) although this ice-core chronology is far more accurate (47 year error) than the GISP2 timescale (Meese et al., 1997) used by Ellison et al. (2006). The thus revised offset would require a shift of the two records relative to one another at the very limit of the combined chronological  $2\sigma$  uncertainty bounds (i.e., well outside the  $1\sigma$  bounds) to make the MD99-2251 *N. pachyderma* (s) event match

**Fig. 6.** Comparison between SL21 *Spiniferites elongatus* (%), GISP2 nss [K<sup>+</sup>], and Qunf Cave  $\delta^{18}\text{O}_{\text{speleothem}}$  through the early to middle Holocene. (a) Relative abundances (%) of *Spiniferites elongatus* in core SL21 with respect to a gonyaulacoid-only dinocyst sum. (b) GISP2 nss [K<sup>+</sup>] (ppb) (grey line). Black solid line represents a 200-year moving Gaussian (Mayewski et al., 1997). (c)  $\delta^{18}\text{O}_{\text{speleothem}}$  (‰, VPDB) from Qunf Cave (Southern Oman) (Fleitmann et al., 2003). Black line represents the Gaussian  $10 \pm 1 \text{ kyr}^{-1}$  bandpass filtering through the early to middle Holocene portion of the record to highlight the long-term (orbital) component of the signal. (d) Detrended Qunf Cave  $\delta^{18}\text{O}_{\text{speleothem}}$  (‰, VPDB) record obtained by removing the long-term (orbital) component from the raw  $\delta^{18}\text{O}_{\text{speleothem}}$  data. Black line represents a 200 years moving average through the detrended record. (e) Lagged cross-correlation analysis between the 200 years moving averages of GISP2 nss [K<sup>+</sup>] and of the detrended Qunf Cave  $\delta^{18}\text{O}_{\text{speleothem}}$  record across the 10.3–8 ka BP interval. Green arrows indicate correlative events discussed in the text. (For interpretation of the references to colour in this figure legend, the reader is referred to the web version of this article.)



the  $\delta^{18}\text{O}_{\text{ice}}$  anomaly in NGRIP and GISP2 (GICC05 timescale). In addition, if the MD99–2251 timescale were ‘shifted’ in such a way that *N. pachyderma* (s) and the  $\delta^{18}\text{O}_{\text{ice}}$  changes come to coincide with one another, then the maximum reduction of ISOW would come to postdate the  $\delta^{18}\text{O}_{\text{ice}}$  anomaly (see Fig. S3). On the other hand, if we assume that the chronology of core MD99–2251 is precise, then the distinct minimum in the bottom-water flow speed would slightly precede the negative shifts in NGRIP and GISP2  $\delta^{18}\text{O}_{\text{ice}}$  (GICC05 timescale), which would agree with the outcome of several model simulations of climate perturbations linked to freshwater-forced AMOC disturbances (e.g., Alley and Ágústsdóttir, 2005; LeGrande et al., 2006; Wiersma and Renssen, 2006).

However, our inference of a precise chronology for core MD99–2251 leaves unaddressed the causal mechanism behind the pronounced MD99–2251 *N. pachyderma* (s) changes prior to the ‘8.2 event’. Noteworthy, a remarkable structural, temporal, and statistical similarity (see Fig. S4 and text in the Supplementary material) is apparent through the 8.6–8.2 interval between the two centennial-scale fluctuations of *N. pachyderma* (s) in core MD99–2251 (Fig. 7d) and the contemporaneous maxima in GISP2 nss  $\text{K}^+$  (GICC05 timescale) (Fig. 7c). This implies that the SST cooling in MD99–2251 likely reflects the broad climatic anomaly that underlies the superimposed sharp  $\delta^{18}\text{O}_{\text{ice}}$  event. The *N. pachyderma* (s) peak at 8.29 ka BP, which predates the most pronounced AMOC reduction seen in the co-registered sortable silt record (Fig. 7e), would then be more a reflection of the underlying repetitive Holocene climate events (Mayewski et al., 2004; Rohling and Pälike, 2005 and references therein) than of the 8.2 ka BP melt-water-induced AMOC reduction.

Contrary to MD99–2251, the co-registered record of MD03–2665 shows cooling and deep-water circulation disturbance at virtually the same time (Fig. 7f and g). Specifically, a reduction in NADW production slightly precedes and spans the sea surface cooling event, in striking agreement with the sequence of events found in climate models (e.g., Alley and Ágústsdóttir, 2005; LeGrande et al., 2006; Wiersma and Renssen, 2006).

### 6.2.3. Early Holocene short-lived climate changes

While the foraminiferal record of LC21 shows signal similarities to GISP2 nss  $[\text{K}^+]$  on multi-centennial to millennial timescales (Rohling et al., 2002), our SL21 *S. elongatus* record shows an even stronger similarity that includes even short centennial-scale events. In particular, there are two sharp *S. elongatus* abundance peaks centred on 8.2 and 8.05 ka BP, which are found superimposed upon a broader period of climatic deterioration in the Aegean Sea between 8.8 and 7.8 ka BP (Fig. 7h). This pattern is highly reminiscent of the underlying multi-centennial climate deterioration with a superimposed abrupt ‘8.2 ka BP event’, as described by Rohling and Pälike (2005). Furthermore, the interval of peak *S. elongatus* abundance appears coeval to the negative 2‰  $\delta^{18}\text{O}_{\text{ice}}$  event in the Greenland ice cores (Fig. 7a) (e.g., Rasmussen et al., 2007), which is thought to represent an  $\sim 6^\circ\text{C}$  cooling of the air temperature over Greenland Summit (Alley et al., 1997). The sharp SL21 *S. elongatus* peaks at 8.2 and 8.05 ka BP also coincide, well within the

chronological confidence limits, with the 8.27–8.07 ka BP minimum in ISOW flow speed (Fig. 7e) (Ellison et al., 2006).

On the basis of these observations we infer that we now have sound evidence for an abrupt winter SST minimum in the Aegean Sea in response to the ‘8.2 ka BP’ AMOC reduction. This finding complements a recent pollen-based reconstruction that suggests particularly harsh winter conditions on the northern Aegean borderlands during the ‘8.2 ka BP event’ (Kotthoff et al., 2008). Importantly, these observations support the outcome of model-based reconstructions of the climatic response of the eastern Mediterranean to AMOC reduction (e.g., LeGrande et al., 2006; Wiersma and Renssen, 2006). Because of the multi-proxy differentiation between the broader underlying climate anomaly and the abrupt true ‘8.2 ka BP event’ in our Aegean records, the event is now identified without ambiguities in the Aegean region.

There are two other early Holocene winter events in the SL21 *S. elongatus* record at 10.5 and 9.5 ka BP (Figs. 5d and 6a), which – within chronological uncertainties – may also correspond to short-lived anomalies that were previously identified in several records from the wider North Atlantic region (Bond et al., 1997; von Grafenstein et al., 1999; Björck et al., 2001; Came et al., 2007; Marshall et al., 2007; Rasmussen et al., 2007) and which may also be related to melt-water-forced reductions of the AMOC (Nesje et al., 2004; Teller and Leverington, 2004; Hillaire-Marcel et al., 2007). For the climate anomaly between 9.3 and 9.2 ka BP (Rasmussen et al., 2007; Fleitmann et al., 2008), which seems to be represented in SL21 by a cooling centred on 9.5 ka BP (Fig. 5), Fleitmann et al. (2008) have proposed a link to a melt-water pulse at St Lawrence Bay (Teller and Leverington, 2004). However, too little is (yet) known about the earliest Holocene events, especially concerning a possible association with AMOC reductions, and the emphasis must be on more widespread and detailed documentation, before any conclusions may be reached.

## 7. Conclusions

Long-term changes in the eastern Mediterranean hydrography are modulated by orbitally driven fluctuations in the African monsoon-fuelled river discharge along the North African margin (Rossignol-Strick et al., 1982; Rohling and Hilgen, 1991; Rohling et al., 2004, 2009; Marino et al., 2007). A  $-1.3\text{‰}$  shift in the  $\delta^{18}\text{O}_{\text{seawater}}$  record for south-eastern Aegean core LC21 between 10.7 and 9.7 ka BP reflects a change to fresher sea surface conditions in the basin in response to the injection, via the Nile River, of isotopically light freshwater. The latter marks the onset of the latest (early Holocene) orbitally driven monsoon maximum over north-eastern Africa. Allowing for chronological uncertainties, this change in SE Aegean  $\delta^{18}\text{O}_{\text{seawater}}$  is contemporaneous to a shift of similar sign and magnitude in the  $\delta^{18}\text{O}_{\text{speleothem}}$  record from Soreq Cave (Northern Israel). This suggests that changes in the isotopic composition of the Aegean–Levantine moisture source may have played an important role in the observed early Holocene changes in Soreq Cave  $\delta^{18}\text{O}_{\text{speleothem}}$ , which may therefore record less

**Fig. 7.** Early Holocene paleoclimate proxy records from Greenland Summit, the northern North Atlantic Ocean, and the Aegean Sea. (a) GISP2 (orange) (Grootes et al., 1993) and NGRIP (black) (Rasmussen et al., 2007)  $\delta^{18}\text{O}_{\text{ice}}$  (‰, VSMOW) on the GICC05 timescale. Horizontal bars represent error uncertainties of the GICC05 (black) and MD99–2251  $^{14}\text{C}$  AMS based (red) chronologies, respectively. (b) GISP2 ss  $[\text{Na}^+]$  (ppb) and (c) GISP2 nss  $[\text{K}^+]$  (ppb) on the GICC05 timescale. Solid line represents the 200-year moving Gaussian (Mayewski et al., 1997). (d) *Neogloboquadrina pachyderma* (s) relative abundances and (e) mean size of sortable silt ( $\mu\text{m}$ ) in core MD99–2251 (Ellison et al., 2006). Solid line represents the 100 year moving averages. Arrows in (e) indicate the directions of stronger (higher mean) and weaker (lower mean) ISOW flows. (f)  $\delta^{18}\text{O}_{\text{pachyderma}}$  (‰, VPDB) and (g)  $\delta^{13}\text{C}_{\text{wuelterstorfi}}$  (‰, VPDB) in core MD03–2665 (Kleiven et al., 2008). Solid line represents a 100 year moving averages. Green bars in (g) indicate the modern North Atlantic Deep Water (NADW, heavier  $\delta^{13}\text{C}$  values) and early Holocene Southern Ocean Water (SOW, lighter  $\delta^{13}\text{C}$  values) end members (Kleiven et al., 2008). (h) Relative abundances (%) of *Spiniferites elongatus* in core SL21 with respect to a gonyaulacoid-only dinocyst sum (blue solid line) and relative abundances (%) of warm-water planktonic foraminifera for core LC21 (orange shaded area; Rohling et al., 2002). Light grey band represents the ‘8.2 event’ in the NGRIP and GISP2  $\delta^{18}\text{O}_{\text{ice}}$ , the dark grey band embeds the central peak event. Black diamond (bottom) indicates the age for the Lake Agassiz drainage event with associated (1 $\sigma$ ) error bars (Barber et al., 1999). (For interpretation of the references to colour in this figure legend, the reader is referred to the web version of this article.)

precipitation increase over Israel than previously considered (Bar-Matthews et al., 2000).

The early Holocene hydrological change in North-East Africa and the associated shift in SE Aegean  $\delta^{18}\text{O}_{\text{seawater}}$  appear to postdate the intensification of the West African monsoon (Sahel) by at least 0.8 kyr (Weldeab et al., 2007), and to be virtually synchronous with a marked shift to wetter condition in Southern Oman, at the present-day northernmost edge of the Indian summer monsoon penetration over the Arabian Peninsula (Fleitmann et al., 2003, 2007). This lagged response of the monsoon front over North-East Africa and the Arabian Peninsula, relative to West Africa, may reflect a time-delay in the development of Saharan vegetation cover (positive vegetation-albedo feedback, Kutzbach et al., 1996; Brovkin et al., 1998) and a delayed removal of the snow cover over the Eurasian continent (negative snow-albedo feedback, Barnett et al., 1988; Fleitmann et al., 2003, 2007; Gupta et al., 2003).

The sensitivity of the Aegean winter climate to variations in the meridional character of the atmospheric polar vortex (Maheras et al., 1999; Rohling et al., 2002; Casford et al., 2003) provides information about superimposed centennial- to millennial-scale changes that were driven by northern high-latitude conditions. We identify two multi-centennial winter SST decreases in our Aegean records, which appear in phase with millennial-scale intensifications of the Siberian High (GISP2 nss  $[\text{K}^+]$ ) at 8.7–8.0 and 6.2–5.0 ka BP, in agreement with a previous study (Rohling et al., 2002). These Aegean SST cooling events range between 1 and 2.5 °C in the south-eastern sector of the basin and are part of repeating pattern of climate fluctuations that recur roughly every 2300 years throughout the Holocene on a global scale (Mayewski et al., 2004). A newly generated SST proxy record from the central Aegean, based on the increases of the cold-water dinocyst *S. elongatus*, shows not only these millennial-scale changes, but also a distinct pattern of shorter, centennial-scale coolings at 10.5, and 9.5–9.03 ka BP. These centennial-scale events share great signal similarity with GISP2 nss  $[\text{K}^+]$ , Indian summer monsoon proxy data, and with several other records from the wider Northern Hemisphere, which suggests the existence of widespread (hemispheric) climatic teleconnections prior to about 8 ka BP, that is, before the development of full interglacial conditions.

The central Aegean *S. elongatus* record also reveals a distinct short-lived (~150 years) cooling event centred on 8.2 ka BP. By employing the new layer-counted GICC05 timescale for both Greenland ice-core  $\delta^{18}\text{O}_{\text{ice}}$  (NGRIP and GISP2) and ion series (GISP2 nss  $[\text{K}^+]$  and ss  $[\text{Na}^+]$ ), we constrain the phasing between a recently published key record of reduced overflow from the Nordic Seas into the northern North Atlantic (Ellison et al., 2006), the Greenland  $\delta^{18}\text{O}_{\text{ice}}$  '8.2 ka BP' event, and the sharp cooling event in the central Aegean Sea at 8.2 ka BP. This exercise demonstrates that both the Greenland  $\delta^{18}\text{O}_{\text{ice}}$  '8.2 ka BP' event and the correlative short cold 'snap' in the central Aegean coincided with a disturbance in North Atlantic deep-water circulation. Thus, our study supports model-based reconstructions of widespread impacts of reduction(s) in the early Holocene Atlantic Meridional Overturning Circulation in response to freshwater release(s) from the retreating Laurentide Ice Sheet, such as the '8.2 ka BP event'.

## Acknowledgements

G.M. was supported by the Department of Biology, Utrecht University and Institute for Coastal Marine Environment, National Research Council (IAMC-CNR) in Naples, Italy. E.J.R. acknowledges financial support from NERC projects NER/B/S/2002/00268, NER/T/S/2002/00453, and NE/D001846/1. Sune Rasmussen provided correlation points to transfer the GISP2 records on the GICC05 timescale. Kikki Kleiven and Dominik Fleitmann have made

available to us their data for core MD03-2665 and Qunf Cave, respectively. Suggestions by Hans Renssen, Walter Finsinger, Oliver Heiri, Bruno D'Argenio, and by three anonymous reviewers were critical for the improvement of the manuscript. We kindly thank Natasja Welters for technical support during palynological processing. This study contributes to the Marine Science and Engineering Doctorate, Federico II University, Naples, Italy.

## Appendix. Supplementary material

Supplementary data associated with this article can be found, in the online version, at doi:10.1016/j.quascirev.2009.08.011.

## References

- Alley, R., Ágústssdóttir, A., 2005. The 8k event: cause and consequences of a major Holocene abrupt climate change. *Quaternary Science Reviews* 24, 1123–1149.
- Alley, R.B., Mayewski, P.A., Sowers, T., Stuiver, M., Taylor, K.C., Clark, P.U., 1997. Holocene climatic instability: a prominent widespread event 8200 years ago. *Geology* 25, 483–486.
- An, Z.S., Porter, S.C., Kutzbach, J.E., Wu, X.H., Wang, S.M., Liu, X.D., Li, X.Q., Zhou, W.J., 2000. Asynchronous Holocene optimum of the East Asian monsoon. *Quaternary Science Reviews* 19, 743–762.
- Ayalon, A., Bar-Matthews, M., Kaufman, A., 1999. Petrography, strontium, barium and uranium concentrations, and strontium and uranium isotope ratios in speleothems as palaeoclimatic proxies: Soreq cave, Israel. *The Holocene* 9 (6), 715–722.
- Barber, D.C., Dyke, A., Hillaire-Marcel, C., Jennings, A.E., Andrews, J.T., Kerwin, M.W., Bilodeau, G., McNeely, R., Southon, J., Morehead, M.D., Gagnon, J.-M., 1999. Forcing of the cold event of 8,200 years ago by catastrophic drainage of Laurentide Lakes. *Nature* 400, 344–348.
- Bar-Matthews, M., Ayalon, A., Kaufman, A., 2000. Timing and hydrological conditions of sapropel events in the eastern Mediterranean, as evident from speleothems, Soreq cave, Israel. *Chemical Geology* 169, 145–156.
- Bar-Matthews, M., Ayalon, A., Kaufman, A., Wasserburg, G., 1999. The eastern Mediterranean paleoclimate as a reflection of regional events: Soreq cave, Israel. *Earth and Planetary Science Letters* 166, 85–95.
- Bar-Matthews, M., Ayalon, A., Matthews, A., Sass, E., Halicz, L., 1996. Carbon and oxygen isotope study of the active water-carbonate system in a karstic Mediterranean cave: implications for paleoclimate research in semiarid regions. *Geochimica et Cosmochimica Acta* 60, 337–347.
- Barnett, T.P., Dumenil, L., Schlese, U., Roeckner, E., 1988. The effect of Eurasian snow cover on global climate. *Science* 239, 504–507.
- Bemis, B.E., Spero, H.J., Bijma, J., Lea, D.W., 1998. Re-evaluation of the oxygen isotopic composition of planktonic foraminifera: experimental results and revised paleotemperature equations. *Paleoceanography* 13, 150–160.
- Björck, S., Muscheler, R., Kromer, B., Andresen, C.S., Heinemeier, J., Johnsen, S.J., Conley, D., Koç, N., Spurk, M., Veski, S., 2001. High-resolution analyses of an early Holocene cooling event may imply decreased solar forcing as an important climate trigger. *Geology* 29, 1107–1110.
- Bond, G., Showers, W., Cheseby, M., Lotti, R., Almasi, P., deMenocal, P., Priore, P., Cullen, H., Hajdas, I., Bonani, G., 1997. A pervasive millennial-scale cycle in north Atlantic Holocene and glacial climates. *Science* 278, 1257–1266.
- Bond, G., Kromer, B., Beer, J., Muscheler, R., Evans, M.N., Showers, W., Hoffmann, S., Lotti-Bond, R., Hajdas, I., Bonani, G., 2001. Persistent solar influence on north Atlantic climate during the Holocene. *Science* 294, 2130–2136.
- Brovkin, V., Claussen, M., Petoukhov, V., Ganopolski, A., 1998. On the stability of the atmosphere-vegetation system in the Sahara/Sahel region. *Journal of Geophysical Research* 103, 31613–31624.
- Came, R.E., Oppo, D.W., McManus, J.F., 2007. Amplitude and timing of temperature and salinity variability in the subpolar north Atlantic over the past 10 k.y. *Geology* 35 (4), 315–318.
- Carlson, A.E., LeGrande, A.N., Oppo, D.W., Came, R.E., Schmidt, G.A., Anslow, F.S., Licciardi, J.M., Obbink, E.A., 2008. Rapid early Holocene deglaciation and sea level rise. *Nature Geoscience* 1, 620–624.
- Casford, J.S.L., Rohling, E.J., Abu-Zied, R.H., Jorissen, F.J., Leng, M., Thomson, J., 2003. A dynamic concept for eastern Mediterranean circulation and oxygenation during sapropel formation. *Palaeogeography, Palaeoclimatology, Palaeoecology* 190, 103–119.
- Casford, J.S.L., Rohling, E.J., Abu-Zied, R.H., Cooke, S., Fontanier, C., Leng, M., Lykousis, V., 2002. Circulation changes and nutrient concentrations in the late Quaternary Aegean Sea: a nonsteady state concept for sapropel formation. *Paleoceanography* 17, 1024. doi:10.1029/2000PA000601.
- Casford, J.S.L., Abu-Zied, R.H., Rohling, E.J., Cooke, S., Fontanier, C., Leng, M., Millard, A., Thomson, J., 2007. A stratigraphically controlled multiproxy chronostratigraphy for the eastern Mediterranean. *Paleoceanography* 22, PA4215. doi:10.1029/2007PA001422.
- Charles, C.D., Rind, D., Jouzel, J., Koster, R.D., Fairbanks, R.G., 1994. Glacial-interglacial changes in moisture sources for Greenland: influence on the ice core record of climate. *Science* 263, 508–511.

- Clark, P.U., Alley, R.B., Pollard, D., 1999. Northern hemisphere ice-sheet influences on global climate change. *Science* 286, 1104–1111.
- Cohen, J., Saito, K., Entekhabi, D., 2001. The role of the Siberian high in northern hemisphere climate variability. *Geophysical Research Letters* 28 (2), 299–302.
- Dansgaard, W., 1964. Stable isotopes in precipitation. *Tellus* 16, 436–468.
- Dansgaard, W., White, J.W.C., Johnsen, S.J., 1989. The abrupt termination of the Younger Dryas climate event. *Nature* 339, 532–534.
- deMenocal, P., Ortiz, J., Guilderson, T., Adkins, J., Sarnthein, M., Baker, L., Yarusinsky, M., 2000. Abrupt onset and termination of the African Humid Period: rapid climate responses to gradual insolation forcing. *Quaternary Science Reviews* 19, 347–361.
- Denton, G.H., Karlén, W., 1973. Holocene climatic variations: their pattern and possible cause. *Quaternary Research* 3, 155–205.
- De Rijk, S., Rohling, E.J., Hayes, A., 1999. Onset of climatic deterioration in the eastern Mediterranean around 7 ky BP: micropalaeontological data from Mediterranean sapropel interruptions. *Marine Geology* 153, 337–343.
- de Vernal, A., Turon, J.-L., Guiot, J., 1994. Dinoflagellate distribution in high-latitude marine environments and quantitative reconstruction of sea-surface salinity, temperature and seasonality. *Canadian Journal of Earth Sciences* 31, 48–62.
- de Vernal, A., Henry, M., Matthiessen, J., Mudie, P.J., Rochon, A., Boessenkool, K.P., Eynaud, F., Grøsfjeld, K., Guiot, J., Hamel, D., Harland, R., Head, M.J., Kunz-Pirring, M., Levac, E., Loucheur, V., Peyron, O., Pospelova, V., Radi, T., Turon, J.-L., Voronina, E., 2001. Dinoflagellate cyst assemblages as tracers of sea-surface conditions in the northern North Atlantic, Arctic and sub-Arctic seas: the new  $n=677$  data base and its application for quantitative palaeoceanographic reconstruction. *Journal of Quaternary Science* 16, 681–698.
- de Vernal, A., Hillaire-Marcel, C., Peltier, W.R., Weaver, A.J., 2002. Structure of the upper water column in the northwest North Atlantic: modern versus Last Glacial Maximum conditions. *Paleoceanography* 17 (4), 1050. doi:10.1029/2001PA000665.
- de Vernal, A., Eynaud, F., Henry, M., Hillaire-Marcel, C., Londeix, L., Mangin, S., Matthiessen, J., Marret, F., Radi, T., Rochon, A., Solignac, S., Turon, J.-L., 2005. Reconstruction of sea surface conditions at middle to high latitudes of the northern hemisphere during the last glacial maximum (LGM) based on dinoflagellate cyst assemblages. *Quaternary Science Reviews* 24, 897–924.
- Dykoski, C.A., Edwards, R.L., Cheng, H., Yuan, D.X., Cai, Y.J., Zhang, M.L., Lin, Y.S., Qing, J.M., An, Z.S., Revenaugh, J., 2005. A high-resolution, absolute-dated Holocene and deglacial Asian monsoon record from Dongge Cave, China. *Earth and Planetary Science Letters* 233, 71–86.
- Ehrmann, W., Schmiedl, G., Hamann, Y., Kuhn, T., Hemleben, C., Siebel, W., 2007. Clay minerals in Lateglacial and Holocene sediments of the northern and southern Aegean Sea. *Paleogeography, Palaeoclimatology, Palaeoecology* 249, 36–57.
- Ellison, C.R.W., Chapman, M.R., Hall, I.R., 2006. Surface and deep ocean interactions during the cold climate event 8200 years ago. *Science* 312, 1929–1932.
- Emeis, K.C., Struck, U., Schulz, H.M., Bernasconi, S., Sakamoto, T., Martinez-Ruiz, F., 2000. Temperature and salinity of Mediterranean Sea surface waters over the last 16,000 years: constraints on the physical environment of S1 sapropel formation based on stable oxygen isotopes and alkenone unsaturation ratios. *Paleogeography, Palaeoclimatology, Palaeoecology* 158, 259–280.
- Facorellis, Y., Maniatis, Y., Kromer, B., 1998. Apparent  $^{14}\text{C}$  ages of marine mollusc shells from a Greek island: calculation of the marine reservoir effect in the Aegean Sea. *Radiocarbon* 40, 963–973.
- Fensome, R.A., Taylor, F.J.R., Norris, G., Sarjeant, W.A.S., Wharton, D.I., Williams, G.L., 1993. A classification of fossil and living dinoflagellates. *Micropaleontology Press Special Publication* 7, 351 pp.
- Fensome, R.A., Williams, G.L., 2004. The Lentin and Williams Index of Fossil Dinoflagellates. In: *AASP Foundation Contributions Series, 2004 Edition, No. 42*, 909 pp.
- Fleitmann, D., Burns, S.J., Mudelsee, M., Bradley, R.S., Kramers, J.D., Matter, A., 2008. A widespread climatic anomaly at around 9200 years before present. *Paleoceanography* 23, PA1102. doi:10.1029/2007PA001519.
- Fleitmann, D., Burns, S.J., Mudelsee, M., Neff, U., Kramers, J., Mangini, A., Matter, A., 2003. Holocene forcing of the Indian monsoon recorded in a stalagmite from Southern Oman. *Science* 300, 1737–1739.
- Fleitmann, D., Burns, S.J., Mangini, A., Mudelsee, M., Kramers, J., Villa, I., Neff, U., Al-Subbary, A.A., Buettner, A., Hippler, D., Matter, A., 2007. Holocene ITCZ and Indian monsoon dynamics recorded in stalagmites from Oman and Yemen (Socotra). *Quaternary Science Reviews* 26, 170–188.
- Fontugne, M., Arnold, M., Labeyrie, L., Paterne, M., Calvert, S.E., Duplessy, J.C., 1994. Palaeoenvironment, sapropel chronology and Nile River discharge during the last 20,000 years as indicated by deep-sea sediment records in the Eastern Mediterranean. *Radiocarbon* 36, 75–88.
- Gasse, F., 2000. Hydrological changes in the African tropics since the Last Glacial Maximum. *Quaternary Science Reviews* 19, 189–211.
- Gertman, I., Pinardi, N., Popov, Y., Hecht, A., 2006. Aegean Sea water masses during the early stages of the Eastern Mediterranean climatic transient (1988–1990). *Journal of Physical Oceanography* 36, 1841–1859.
- Goodfriend, G.A., 1991. Holocene trends in  $^{18}\text{O}$  in land snail shells from the Negev Desert and their implications for changes in rainfall source areas. *Quaternary Research* 35, 417–426.
- Groote, P.M., Stuiver, M., White, J.W.C., Johnsen, S.J., Jouzel, J., 1993. Comparison of oxygen isotope records from the GISP2 and GRIP Greenland ice cores. *Nature* 366, 552–554.
- Gupta, A.K., Anderson, D.M., Overpeck, J.T., 2003. Abrupt changes in the Asian southwest monsoon during the Holocene and their links to the North Atlantic Ocean. *Nature* 421, 354–357.
- Hansen, B., Østerhus, S., 2000. North Atlantic – Nordic seas exchanges. *Progress in Oceanography* 45, 109–208.
- Hansen, B., Turrell, W.R., Østerhus, S., 2001. Decreasing overflow from the Nordic seas into the Atlantic Ocean through the Faroe bank channel since 1950. *Nature* 411, 927–930.
- Hayes, A., Rohling, E.J., De Rijk, S., Zachariasse, W.J., 1999. Mediterranean planktonic foraminiferal faunas during the last glacial cycle. *Marine Geology* 153, 239–252.
- Hayes, A., Kucera, M., Kallel, N., Sbaffi, L., Rohling, E.J., 2005. Glacial Mediterranean sea surface temperatures based on planktonic foraminiferal assemblages. *Quaternary Science Reviews* 24 (7–9), 999–1016.
- Haug, G.H., Hughen, K.A., Sigman, D.M., Peterson, L.C., Rohl, U., 2001. Southward migration of the intertropical convergence zone through the Holocene. *Science* 293, 1304–1308.
- Hillaire-Marcel, C., de Vernal, A., Piper, D.J.W., 2007. Lake Agassiz final drainage event in the northwest North Atlantic. *Geophysical Research Letters* 34, L15601.
- Hughen, K.A., Baillie, M.G.L., Bard, E., Bayliss, A., Beck, J.W., Bertrand, C., Blackwell, P.G., Buck, C.E., Burr, G., Cutler, K.B., Damon, P.E., Edwards, R.L., Fairbanks, R.G., Friedrich, M., Guilderson, T.P., Kromer, B., McCormac, F.G., Manning, S., Bronk Ramsey, C., Reimer, P.J., Reimer, R.W., Remmele, S., Southon, J.R., Stuiver, M., Talamo, S., Taylor, F.W., van der Plicht, J., Weyhenmeyer, C.E., 2004. Marine04 marine radiocarbon age calibration, 0–26 cal kyr BP. *Radiocarbon* 46 (3), 1059–1086.
- Hunter, S., Wilkinson, D., Louarn, E., McCave, N., Rohling, E.J., Stow, D., Bacon, S., 2007. Deep western boundary current dynamics and associated sedimentation on the Eirik Drift, southern Greenland margin. *Deep-Sea Research I* 54, 2036–2066.
- Kleiven, H.F., Catherine, K., Laj, C., Ninnemann, U.S., Richter, T.O., Cortijo, E., 2008. Reduced North Atlantic deep water coeval with the glacial Lake Agassiz freshwater outburst. *Science* 319, 60–64.
- Kotthoff, U., Pross, J., Müller, U.C., Peyron, O., Schmiedl, G., Schulz, H., Bordon, A., 2008. Climate dynamics in the borderlands of the Aegean Sea during formation of Sapropel S1 deduced from a marine pollen record. *Quaternary Science Reviews* 27, 832–845.
- Kucera, M., Rosell-Melè, A., Schneider, R., Waelbroeck, C., Weinelt, M., 2005. Multiproxy approach for the reconstruction of the glacial ocean surface (MARGO). *Quaternary Science Reviews* 24 (7–9), 813–819.
- Kuhn, T., Schmiedl, G., Ehrmann, W., Hamann, Y., Hemleben, C., 2007. Deep-sea ecosystem variability of the Aegean Sea during the past 22 kyr as revealed by benthic foraminifera. *Marine Micropaleontology* 64, 141–162.
- Kutzbach, J.E., Bonan, G., Foley, J., Harrison, S.P., 1996. Vegetation and soil feedbacks on the response of the African monsoon to orbital forcing in the early to middle Holocene. *Nature* 384, 623–626.
- Laskar, J., 1990. The chaotic motion of the solar system. A numerical estimate of the size of the chaotic zones. *Icarus* 88, 266–291.
- LeGrande, A.N., Schmidt, G.A., Shindell, D.T., Field, C.V., Miller, R.L., Koch, D.M., Faluvegi, G., Hoffmann, G., 2006. Consistent simulations of multiple proxy responses to an abrupt climate change event. *Proceedings of the National Academy of Sciences* 103, 837–842.
- Lionello, P., Malanotte-Rizzoli, P., Boscolo, R., Alpert, P., Artale, V., Li, L., Luterbacher, J., May, W., Trigo, R., Tsimplis, M., Ulbrich, U., Xoplaki, E., 2006. The Mediterranean climate: an overview of the main characteristics and issues. In: Lionello, P., Malanotte-Rizzoli, P., Boscolo, R. (Eds.), *Mediterranean Climate Variability*. Elsevier, Amsterdam, The Netherlands, pp. 1–26.
- Lykousis, V., Chronis, G., Tselepidis, A., Price, N.B., Theocharis, A., Siokou-Frangou, I., Van Wambeke, F., Danovaro, R., Stavrakakis, S., Duineveld, G., Georgopoulos, D., Ignatiades, L., Souvermezoglou, A., Voutsinou-Taliadouri, F., 2002. Major outputs of the recent multidisciplinary biogeochemical researches undertaken in the Aegean Sea. *Journal of Marine Science* 33–34, 313–334.
- Maasch, K.A., Mayewski, P.A., Rohling, E.J., Stager, J.C., Karlen, W., Meeker, L.D., Meyerson, E.A., 2005. A 2000 year context for modern climate change. *Geografiska Annaler* 87A, 7–15.
- Maheras, P., Xoplaki, E., Davies, T., Martin-Vide, J., Bariendos, M., Alcoforado, M.J., 1999. Warm and cold monthly anomalies across the Mediterranean basin and their relationship with circulation; 1860–1990. *International Journal of Climatology* 19, 1697–1715.
- Malmgren, B.A., Kucera, M., Nyberg, J., Waelbroeck, C., 2001. Comparison of statistical and artificial neural network techniques for estimating past sea-surface temperatures from planktonic foraminifer census data. *Paleoceanography* 16 (5), 520–530.
- Mangini, A., Verdes, P., Spötl, C., Scholz, D., Vollweiler, N., Kromer, B., 2007. Persistent influence of the North Atlantic hydrography on central European winter temperature during the last 9000 years. *Geophysical Research Letters* 34, L02704.
- Marino, G., Rohling, E.J., Rijpstra, W.I., Sangiorgi, F., Schouten, S., Sinninghe Damsté, J.S., 2007. The Aegean Sea as driver of hydrographic and ecological changes in the eastern Mediterranean. *Geology* 35 (8), 675–678.
- Marret, F., Zonneveld, K.A.F., 2003. Atlas of modern organic-walled dinoflagellate cyst distribution. *Review of Palaeobotany and Palynology* 125, 1–200.
- Marshall, J.D., Lang, B., Crowley, S.F., Weedon, G.P., van Calsteren, P., Fisher, E.H., Holme, R., Holmes, J.A., Jones, R.T., Bedford, A., Brooks, S.J., Bloemendal, J.,

- Kiriakoulakis, K., Ball, J.D., 2007. Terrestrial impact of abrupt changes in the North Atlantic thermohaline circulation: early Holocene, UK. *Geology* 35 (7), 639–642.
- Matthews, A., Ayalon, A., Bar-Matthews, M., 2000. D/H ratios of fluid inclusions of Soreq Cave (Israel) speleothems as a guide to the eastern Mediterranean meteoric line relationships in the last 120 ky. *Chemical Geology* 166, 183–191.
- Mayewski, P.A., Meeker, L.D., Twickler, M.S., Whitlow, S., Yang, Q., Lyons, W.B., Prentice, M., 1997. Major features and forcing of high-latitude northern hemisphere atmospheric circulation using a 110,000-year long glaciochemical series. *Journal of Geophysical Research* 102 (C12), 26345–26366.
- Mayewski, P.A., Rohling, E.J., Stager, J.C., Karlen, W., Maasch, K.A., Meeker, L.D., Meyerson, E.A., Gasse, F., van Kreveld, S., Holmgren, K., Lee-Thorp, J., Rosqvist, G., Rack, F., Staubwasser, M., Schneider, R.R., Steig, E., 2004. Holocene climate variability. *Quaternary Research* 62, 243–255.
- McGarry, S., Bar-Matthews, M., Matthews, A., Vaks, A., Schilman, B., Ayalon, A., 2004. Constraints on hydrological and paleotemperature variations in the eastern Mediterranean region in the last 140 ka given by the  $\delta D$  values of speleothem fluid inclusions. *Quaternary Science Reviews* 23, 919–934.
- MEDAR Group, 2002. MEDATLAS/2002 database. Mediterranean and Black Sea database of temperature salinity and bio-chemical parameters. In: *Climatological Atlas*. IFREMER Edition (4 Cdroms).
- Meese, D.A., Gow, A.J., Alley, R.B., Zielinski, G.A., Grootes, P.M., Ram, M., Taylor, K.C., Mayewski, P.A., Bolzan, J.F., 1997. The Greenland Ice Sheet Project 2 depth-age scale: methods and results. *Journal of Geophysical Research* 102 (C12), 26411–26424.
- Meeker, L.D., Mayewski, P.A., 2002. A 1400-year high-resolution record of atmospheric circulation over the North Atlantic and Asia. *The Holocene* 12, 257–266.
- Mercone, D., Thomson, J., Abu-Zied, R.H., Croudace, I.W., Rohling, E.J., 2001. High resolution geochemical and micropalaeontological profiling of the most recent eastern Mediterranean sapropel. *Marine Geology* 177, 25–44.
- Mercone, D., Thomson, J., Croudace, I.W., Siani, G., Paterne, M., Troelstra, S., 2000. Duration of S1, the most recent sapropel in the eastern Mediterranean Sea, as indicated by accelerator mass spectrometry radiocarbon and geochemical evidence. *Paleoceanography* 15, 336–347.
- Neff, U., Burns, S.J., Mangini, A., Mudelsee, M., Fleitmann, D., Matter, A., 2001. Strong coherence between solar variability and the monsoon in Oman between 9 and 6 ka ago. *Nature* 411, 290–293.
- Nesje, A., Dahl, S.O., Bakke, J., 2004. Were abrupt Lateglacial and early-Holocene climatic changes in northwest Europe related to freshwater outbursts to the North Atlantic and Arctic oceans? *The Holocene* 14, 299–310.
- NGRIP members, 2004. High-resolution record of northern hemisphere climate extending into the Last Interglacial period. *Nature* 431, 147–151.
- O'Brien, S.R., Mayewski, P.A., Meeker, L.D., Meese, D.A., Twickler, M.S., Whitlow, S.E., 1995. Complexity of Holocene climate as reconstructed from a Greenland ice core. *Science* 270, 1962–1964.
- Osborne, A.H., Vance, D., Rohling, E.J., Barton, N., Rogerson, M., Fello, N., 2008. A humid corridor across the Sahara for the migration “Out of Africa” of early modern humans 120,000 years ago. *Proceedings of the National Academy of Sciences* 105, 16444–16447.
- Overpeck, J., Anderson, D., Trumbore, S., Prell, 1996. The southwest Indian monsoon over the last 18,000 years. *Climate Dynamics* 12, 213–225.
- Paillard, D., Labeyrie, L., Yiou, P., 1996. Macintosh program performs time-series analysis. EOS, *Transactions, American Geophysical Union* 77, 379.
- Pinardi, N., Masetti, E., 2000. Variability of the large scale general circulation of the Mediterranean Sea from observations and modelling: a review. *Palaeogeography, Palaeoclimatology, Palaeoecology* 158, 153–173.
- Poulos, S.E., Drakopoulos, P.G., Collins, M.B., 1997. Seasonal variability in sea surface oceanographic conditions in the Aegean Sea (eastern Mediterranean): an overview. *Journal of Marine Systems* 13, 225–244.
- Ramel, R., Gallee, H., Messenger, C., 2006. On the northward shift of the West African monsoon. *Climate Dynamics* 26, 429–440.
- Rasmussen, S.O., Vinther, B.M., Clausen, H.B., Andersen, K.K., 2007. Early Holocene climate oscillations recorded in three Greenland ice cores. *Quaternary Science Reviews* 26, 1907–1914.
- Rasmussen, S.O., Seierstad, I.K., Andersen, K.K., Bigler, M., Dahl-Jensen, D., Johnsen, S.J., 2008. Synchronization of the NGRIP, GRIP, and GISP2 ice cores across MIS 2 and palaeoclimatic implications. *Quaternary Science Reviews* 27 (1–2), 18–28.
- Reimer, P.J., McCormac, F.G., 2002. Marine radiocarbon reservoir corrections for the Mediterranean and Aegean Seas. *Radiocarbon* 44, 159–166.
- Ritchie, J.C., Eyles, C.H., Haynes, C.V., 1985. Sediment and pollen evidence for an early to mid-Holocene humid period in the eastern Sahara. *Nature* 314, 352–355.
- Rochon, A., de Vernal, A., Turon, J.-L., Matthiessen, J., Head, M.J., 1999. Distribution of dinoflagellate cyst assemblages in surface sediments from the North Atlantic Ocean and adjacent basins and quantitative reconstruction of sea-surface parameters. *Special Contribution Series of the American Association of Stratigraphic Palynologists* 35, Dallas, TX, USA.
- Rodwell, M.J., Hoskins, B.J., 1996. Monsoons and the dynamics of deserts. *The Quarterly Journal of the Royal Meteorological Society* 122, 1385–1404.
- Rohling, E.J., 1999. Environmental control on Mediterranean salinity and  $\delta^{18}O$ . *Paleoceanography* 14, 706–715.
- Rohling, E.J., De Rijk, S., 1999. The Holocene climate optimum and Last Glacial Maximum in the Mediterranean: the marine oxygen isotope record. *Marine Geology* 153, 57–75.
- Rohling, E.J., Hilgen, F.J., 1991. The eastern Mediterranean climate at times of sapropel formation: a review. *Geologie en Mijnbouw* 70, 253–264.
- Rohling, E.J., Pälike, H., 2005. Centennial-scale climate cooling with a sudden cold event around 8,200 years ago. *Nature* 434, 975–979.
- Rohling, E.J., Mayewski, P.A., Hayes, A., Abu-Zied, R.H., Casford, J.S.L., 2002. Holocene atmosphere–ocean interactions: records from Greenland and the Aegean Sea. *Climate Dynamics* 18, 587–593.
- Rohling, E.J., Abu-Zied, R.H., Casford, J.S.L., Hayes, A., Hoogakker, B.A.A., 2009. The marine environment: present and past. In: Woodward, J.C. (Ed.), *The Physical Geography of the Mediterranean*. Oxford University Press, Oxford, UK, pp. 33–67.
- Rohling, E.J., Sprovieri, M., Cane, T.R., Casford, J.S.L., Cooke, S., Bouloubassi, I., Emeis, K.C., Schiebel, R., Hayes, A., Jorissen, F.J., Kroon, D., 2004. Reconstructing past planktic foraminiferal habitats using stable isotope data: a case history for Mediterranean sapropel S5. *Marine Micropaleontology* 50, 89–123.
- Rosignol-Strick, M., Nesteroff, V., Olive, P., Vergnaud-Grazzini, C., 1982. After the deluge; Mediterranean stagnation and sapropel formation. *Nature* 295, 105–110.
- Sangiorgi, F., Capotondi, L., Brinkhuis, H., 2002. A centennial scale organic-walled dinoflagellate cyst record of the last deglaciation in the South Adriatic Sea (Central Mediterranean). *Palaeogeography, Palaeoclimatology, Palaeoecology* 186, 199–216.
- Sangiorgi, F., Capotondi, L., Combourieu Nebout, N., Vigliotti, L., Brinkhuis, H., Giunta, S., Lotter, A.F., Morigi, C., Negri, A., Reichart, G.-J., 2003. Holocene seasonal sea-surface temperature variations in the southern Adriatic Sea inferred from a multiproxy approach. *Journal of Quaternary Science* 18, 723–732.
- Scriver, A., Vance, D., Rohling, E.J., 2004. New neodymium isotope data quantify Nile involvement in Mediterranean anoxic episodes. *Geology* 32, 565–568.
- Siani, G., Paterne, M.E., Sulpizio, R., Sbrana, A., Arnold, M., Haddad, G., 2001. Mediterranean Sea surface radiocarbon reservoir age changes since the Last Glacial Maximum. *Science* 294, 1917–1920.
- Sperling, M., Schmiedl, G., Hemleben, C., Emeis, K.-C., Erlenkeuser, H., Grootes, P.M., 2003. Black Sea impact on formation of eastern Mediterranean sapropel S1? Evidence from the Marmara Sea. *Palaeogeography, Palaeoclimatology, Palaeoecology* 190, 9–21.
- Stuiver, M., Reimer, P.J., 1993. Extended  $^{14}C$  database and revised CALIB 3.0  $^{14}C$  age calibration program. *Radiocarbon* 35, 215–230.
- Taylor, F.J.R., 1987. *The Biology of Dinoflagellates*. In: *Botanical Monographs*, vol. 21. Blackwell Scientific Publications, London, UK, 785 pp.
- Teller, J.T., Leverington, D.W., 2004. Glacial Lake Agassiz: a 5000 yr history of change and its relationship to the  $\delta^{18}O$  record of Greenland. *Geological Society of America Bulletin* 116, 729–742.
- Thomas, E.R., Wolff, E.W., Mulvaney, R., Steffensen, J.P., Johnsen, S.J., Arrowsmith, C., White, J.W.C., Vaughn, B., Popp, T., 2007. The 8.2 ka event from Greenland ice cores. *Quaternary Science Reviews* 26, 70–81.
- Versteegh, G.J.M., Zonneveld, K.A.F., 2002. Use of selective degradation to separate preservation from productivity. *Geology* 30 (7), 615–618.
- von Grafenstein, U., Erlenkeuser, H., Brauer, A., Jouzel, J., Johnsen, S., 1999. A mid-European decadal isotope–climate record from 15,500 to 5,000 years BP. *Science* 284, 1654–1657.
- Waelbroeck, C., Labeyrie, L., Michel, E., Duplessy, J.C., McManus, J.F., Lambeck, K., Balbon, E., Labracherie, M., 2002. Sea-level and deep water temperature changes derived from benthonic foraminifera isotopic records. *Quaternary Science Reviews* 21, 295–305.
- Webster, P.J., Magana, V.O., Palmer, T.N., Shukla, J., Tomas, R.A., Yanai, M., Yasunari, T., 1998. Monsoons: processes, predictability, and the prospects for prediction. *Journal of Geophysical Research: Oceans* 103, 14451–14510.
- Weldeab, S., Lea, D.W., Schneider, R.R., Andersen, N., 2007. 155,000 years of West African monsoon and ocean thermal evolution. *Science* 316, 1303–1307.
- Wiersma, A.P., Renssen, H., 2006. Model–data comparison for the 8.2 ka BP event: confirmation of a forcing mechanism by catastrophic drainage of Laurentide Lakes. *Quaternary Science Reviews* 25, 63–88.
- Zervakis, V., Georgopoulos, D., Karageorgis, A.P., Theocharis, A., 2004. On the response of the Aegean Sea to climatic variability: a review. *International Journal of Climatology* 24, 1845–1858.
- Ziv, B., Saaroni, H., Alpert, P., 2004. The factors governing the summer regime of the eastern Mediterranean. *International Journal of Climatology* 24, 1859–1871.
- Zonneveld, K.A.F., 1995. Palaeoclimatic and paleo-ecologic changes during the last deglaciation in the Eastern Mediterranean; implications for dinoflagellate ecology. *Review of Palaeobotany and Palynology* 84 (3), 221–253.
- Zonneveld, K.A.F., 1996. Palaeoclimatic reconstruction of the last deglaciation (18 ka B.P.–8 ka B.P.) in the Adriatic Sea region: a land–sea correlation based on palynological evidence. *Palaeogeography, Palaeoclimatology, Palaeoecology* 122, 89–106.
- Zonneveld, K.A.F., Versteegh, G.J.M., de Lange, G.J., 2001. Palaeo-productivity and postdepositional aerobic organic matter decay reflected by dinoflagellate cyst assemblages of the Eastern Mediterranean S1 sapropel. *Marine Geology* 172, 181–195.
- Zonneveld, K.A.F., Bockelmann, F., Holzwarth, U., 2007. Selective aerobic degradation of organic walled dinoflagellates as tool to quantify past net primary production and bottom water oxygen concentrations. *Marine Geology* 237 (3–4), 109–126.